iScience

CellPress
OPEN ACCESS

Article

Glycogenolysis Is Crucial for Astrocytic Glycogen Accumulation and Brain Damage after Reperfusion in Ischemic Stroke

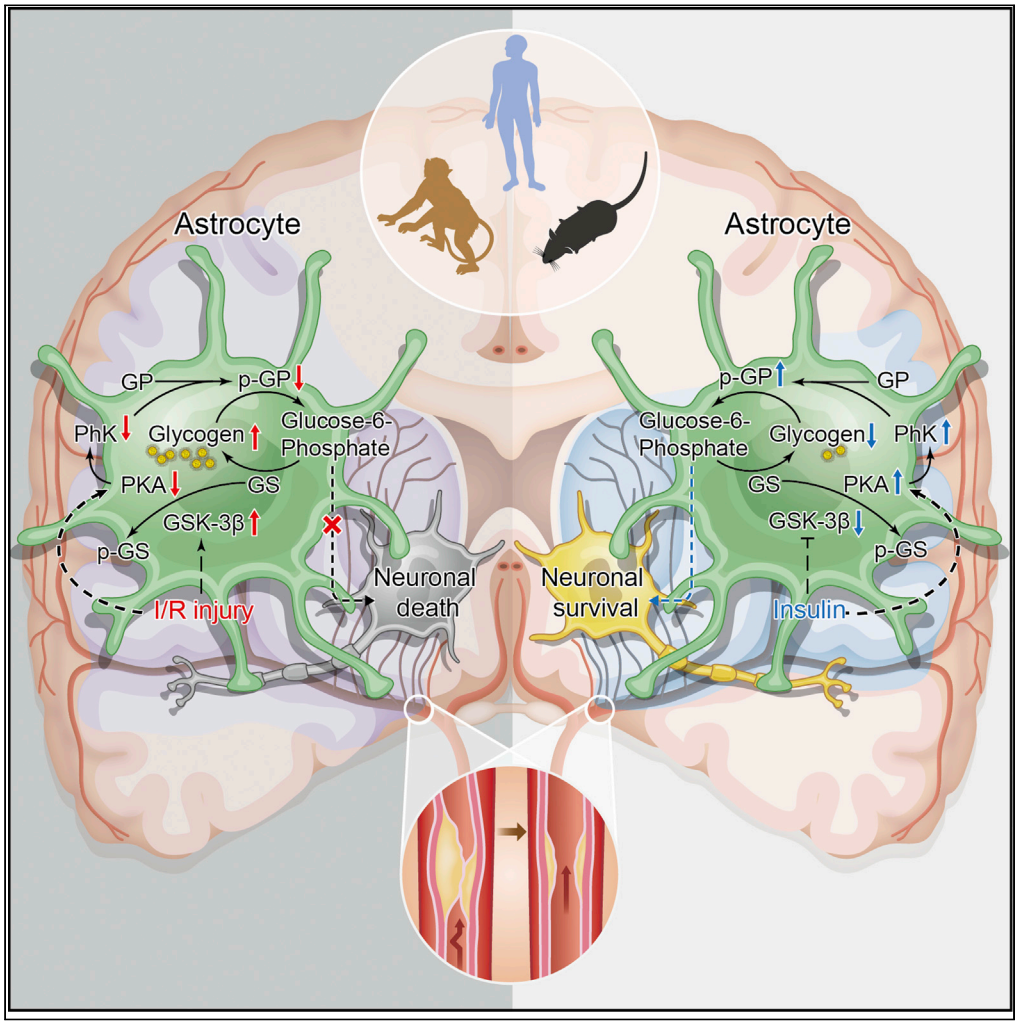

Yanhui Cai, Haiyun Guo, Ze Fan, ..., Hailong Dong, Yan Li, Lize Xiong

liyanxjtu@xjtu.edu.cn (Y.L.)
mzkxlz@126.com (L.X.)

HIGHLIGHTS

Glycogen accumulates upon cerebral reperfusion in humans, primates, and rodents

Impaired glycogenolysis underlies excess glycogen during cerebral reperfusion

Activating glycogenolysis protects against acute and subacute reperfusion insult

Insulin mediates neuroprotection partly by rescuing glycogenolysis upon reperfusion

Cai et al., iScience 23, 101136
May_22, 2020
https://doi.org/10.1016/j.isci.2020.101136

iScience

CellPress
OPEN ACCESS

Article

Glycogenolysis Is Crucial for Astrocytic Glycogen Accumulation and Brain Damage after Reperfusion in Ischemic Stroke

Yanhui Cai,[1,6] Haiyun Guo,[1,6] Ze Fan,[1,6] Xinlei Zhang,[2,6] Di Wu,[3] Wenhong Tang,[1] Tingting Gu,[1] Shiquan Wang,[1] Anqi Yin,[1] Liang Tao,[1] Xunming Ji,[3] Hailong Dong,[1] Yan Li,[4,*] and Lize Xiong[1,5,7,*]

SUMMARY

Astrocytic glycogen is an important energy reserve in the brain and is believed to supply fuel during energy crisis. However, the pattern of glycogen metabolism in ischemic stroke and its potential therapeutic impact on neurological outcomes are still unknown. Here, we found extensive brain glycogen accumulation after reperfusion in ischemic stroke patients and primates. Glycogenolytic dysfunction in astrocytes is responsible for glycogen accumulation, caused by inactivation of the protein kinase A (PKA)-glycogen phosphorylase kinase (PhK)-glycogen phosphorylase (GP) cascade accompanied by the activation of glycogen synthase kinase-3β (GSK3β). Genetic or pharmacological augmentation of astrocytic GP could promote astrocyte and neuron survival and improve neurological behaviors. In addition, we found that insulin exerted a neuroprotective effect, at least in part by rescuing the PKA-PhK-GP cascade to maintain homeostasis of glycogen metabolism during reperfusion. Together, our findings suggest a promising intervention for undesirable outcomes in ischemic stroke.

INTRODUCTION

Stroke is the leading cause of mortality and disability in the adult population (GBD, 2015 DALYs and HALE Collaborators, 2016; GBD, 2015Mortality and Causes of Death Collaborators, 2016), and approximately 70% of all strokes are ischemic strokes (Hankey, 2017). Restoration of blood flow to the brain with thrombolysis or endovascular thrombectomy after ischemic stroke onset is the most effective therapeutic strategy to reduce the infarct region and salvage the cells in the ischemic penumbra (Ma et al., 2019). However, reperfusion itself contributes to cerebral injury and greatly increases the incidence of cerebral edema and hemorrhagic transformation (Bar and Biller, 2018). Blood deficiency and resupply during ischemia/reperfusion (I/R) disrupts brain energy homeostasis, which inevitably aggravates glutamate excitotoxicity, calcium overload, free radical formation, and inflammation, known as the traditional underlying mechanisms of I/R injury (Krewson et al., 2020; Pundik et al., 2012).

The brain accounts for only 2% of the body weight but consumes 20% of the energy of the whole body (Magistretti and Allaman, 2015). Thus, slight energy deficiency in the brain causes severe dysfunction. Glycogen is the only endogenous energy reserve for the brain during cerebrovascular obstruction and is steadily and dynamically maintained through the balance between glycogenesis and glycogenolysis (Bak et al., 2018). Glycogen synthase kinase-3 (GSK3) and protein kinase A (PKA) comodulate the activity of glycogen synthase (GS), the rate-limiting enzyme in glycogenesis (Zois and Harris, 2016). Glycogen phosphorylase (GP), the key enzyme in glycogenolysis, is controlled by the PKA-glycogen phosphorylase kinase (PhK) cascade (Zois and Harris, 2016). Glycogen is mainly located in astrocytes, but recently, very sensitive assays revealed that it exists in small amounts in neurons with active glycogen metabolism (Duran et al., 2019; Saez et al., 2014). Glycogen plays important roles in astrocyte energetics, including pumping Ca^{2+} into the endoplasmic reticulum (ER) controlling the extracellular K^+ concentration and managing oxidative stress (Dienel, 2019; Dienel and Cruz, 2015). In addition, the stored glycogen in astrocytes can be rapidly triggered to generate metabolic support for neighboring neurons by switching astrocytic glycolysis from blood-borne glucose to glycogen, which spares an equivalent amount of blood-borne glucose for neurons (Dienel and Rothman, 2019). However, little is known about the alterations in glycogen metabolism that occur during recanalization and their impacts on neurological outcomes after ischemic stroke.

[1]Department of Anesthesiology and Perioperative Medicine, Xijing Hospital, Fourth Military Medical University, Xi'an, Shaanxi 710032, China

[2]Department of Medicinal Chemistry, School of Pharmacy, Fourth Military Medical University, Xi'an, Shaanxi 710032, China

[3]China-America Institute of Neuroscience, Xuanwu Hospital, Capital Medical University, Beijing 100053, China

[4]Center for Brain Science & Department of Anesthesiology, The First Affiliated Hospital of Xi'an Jiaotong University, Xi'an, Shaanxi 710061, China

[5]Translational Research Institute of Brain and Brain-Like Intelligence & Department of Anesthesiology and Perioperative Medicine, Shanghai Fourth People's Hospital Affiliated to Tongji University School of Medicine, Shanghai 200081, China

[6]These authors contributed equally

[7]Lead Contact

*Correspondence: liyanxjtu@xjtu.edu.cn (Y.L.), mzkxlz@126.com (L.X.)

https://doi.org/10.1016/j.isci.2020.101136

Here, we provide evidence that strongly suggests glycogen accumulation at the onset of reperfusion is associated with the development of I/R injury in stroke patients and animal models. In addition, dysfunction of the PKA-PhK-GP cascade is involved in glycogenolytic reprogramming in astrocytes. Genetic and pharmacological augmentation of glycogen breakdown during recirculation could rescue astrocyte and cocultured neuron survival and improve neurological outcomes after ischemic stroke. In addition, we found that insulin exhibits neuroprotective effects, at least in part by rescuing the PKA-PhK-GP cascade to maintain homeostasis of glycogen metabolism during reperfusion.

RESULTS

Glycogen Accumulates in the Human, Primate, and Rodent Brain during Recanalization after Ischemia

Firstly, we conducted studies on brain tissues from 4 stroke patients who received thrombolytic treatment within 6 h after the onset of stroke. The postmortem interval was approximately 30–40 min, and the interval between thrombolysis and death for these patients ranged from 11 h to 14 h (Table S1). A schematic of the penumbra in the ipsilateral hemisphere and the homologous region in the contralateral hemisphere was shown in Figure 1A (top panel). The levels of glycogen significantly increased in the penumbra compared with the contralateral region after recanalization in stroke patients, as indicated by periodic acid-Schiff (PAS) staining and biochemical assays (Figure 1A, bottom and right panel). Glycogen accumulation was also observed in monkey and mouse brains at 12 h after reperfusion (Figure 1A, bottom and right panel), indicating that reperfusion-induced glycogen accumulation is common across species. The oxygen-glucose deprivation/reoxygenation (OGD/R) model was further used to mimic I/R stress *in vitro*. Consistent with the results obtained *in vivo*, extensive glycogen accumulation was observed in cultured astrocytes *in vitro* after OGD/R, as demonstrated by PAS staining and biochemical assays (Figure 1B). In addition, cellular localization was investigated using electron microscopy, and we observed that a large amount of glycogen was mainly distributed in astrocytes but not neurons at 12 h in the mouse I/R model (Figure 1C).

Next, dynamic changes in glycogen accumulation were investigated separately using electron microscopy and biochemical assays. Glycogen granule levels began to increase 2 h after reperfusion, peaked at 12 h, and accumulated for at least 72 h in the mouse model of middle cerebral artery occlusion/reperfusion (MCAO/R) (Figures 2A–2C). Consistent with these *in vivo* data, glycogen levels were substantially elevated in cultured astrocytes after OGD/R (Figures 2D–2F). The glycogen levels in cultured astrocytes began to increase 6 h after reoxygenation, were at least two-fold higher than the initial levels at 12 h and remained elevated for at least 72 h in the OGD/R model (Figures 2E and 2F). In addition, we observed that glycolytic capacity was inhibited and ATP production decreased at 12 h after reperfusion in the cultured astrocytes (Figure S1).

Dysfunction of Astrocytic GP Is Responsible for the Extensive Glycogen Accumulation Caused by Suppression of PKA/PhK

The basal glycogen levels in astrocytes depend on the balance between glycogenesis and glycogenolysis (Brewer and Gentry, 2019). We first detected the expression of key enzymes in glycogenesis and glycogenolysis in cultured astrocytes. In addition to GS, glycogen branching enzyme (GBE1) plays a role in cerebral glycogenesis to some extent (Brewer and Gentry, 2019). We found that the mRNA and protein levels of GS and GBE1 were relatively stable at different time points during OGD/R stress (Figures 3A, 3B, S2A, and S2B). GP has three isoforms in the brain: PYGB (brain isoform of GP), PYGM (muscle isoform of GP), and PYGL (liver isoform of GP) (Brewer and Gentry, 2019), and we found the mRNA proportion of PYGB, PYGM, and PYGL was 91.7%, 6.1%, and 2.2% in cultured astrocytes, respectively (Figure S2C). The changes in the protein and mRNA levels of PYGB, PYGM, and PYGL during OGD/R are presented in Figures 3C–3E and S2D–S2F. Protein level was lowest for PYGB at 12 h, when its mRNA expression was also half of the normal level (Figures 3C and S2D). Both the mRNA and protein levels of glycogen debranchingenzyme (AGL), another key enzyme in glycogenolysis, showed no significant changes (Figures 3F and S2G). Subsequently, we investigated the activity of GS and GP. The activity of GS was not markedly affected after reoxygenation, as determined by biochemical analysis (Figure 3G). However, total GP activity was decreased at 12 h after reoxygenation according to a biochemical assay (Figure 3H).

The next question is why GP, but not GS, is dysfunctional during I/R. Previous evidence has suggested that the PKA-PhK-GP pathway controls glycogen degradation and that both PKA and GSK3 can inhibit the

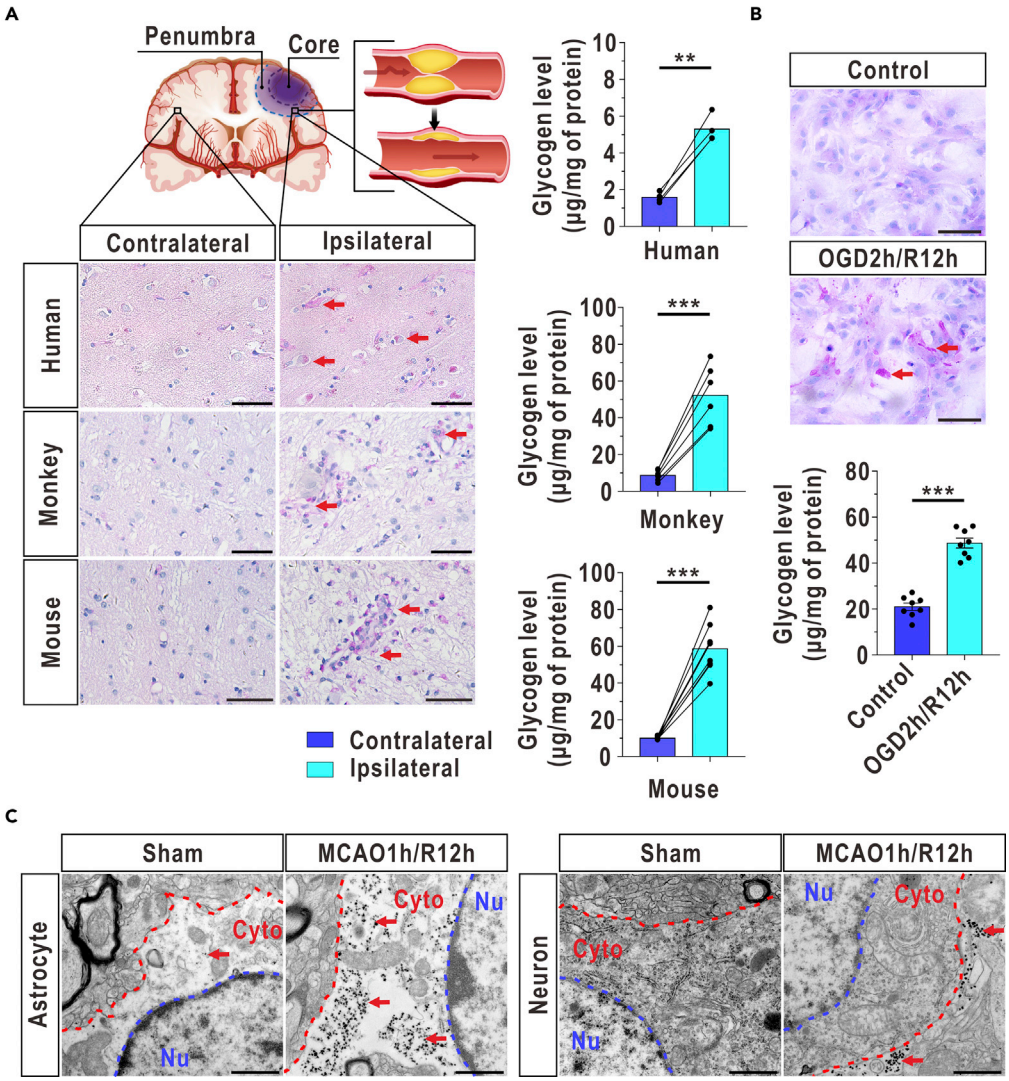

Figure 1. Cerebral Glycogen Is Substantially Increased in Human, Primate, Rodent, and Cultured Astrocytes at the Onset of Reperfusion

(A) A representative diagram showing the core infarct and penumbral regions in the ipsilateral hemisphere after I/R onset (top). Glycogen accumulated in the ischemic penumbra of the ipsilateral hemisphere compared with the contralateral hemisphere in humans (n = 4, paired samples ttest), monkeys (n = 6, paired samples ttest, at 12 h after reperfusion), and mice (n = 8, paired samples ttest, at 12 h after reperfusion) after reperfusion, as indicated by PAS staining. The glycogen levels in the ischemic penumbra of the ipsilateral hemisphere and the homologous contralateral hemisphere were quantified with a biochemical assay. The arrows indicate glycogen-positive cells. Scale bars represent 50 μm.

(B) Increased glycogen in cultured astrocytes, as revealed by PAS staining and a biochemical assay at 12 h after reoxygenation (n = 8, independent ttest). The arrows indicate glycogen-positive cells. Scale bars represent 100 μm.

(C) Excessively elevated glycogen was localized in astrocytes but not neurons at 12 h after reperfusion in the mouse brain, as revealed using electron microscopy. The arrows indicate glycogen granules. Nu represents the nucleus. Cyto represents the cytoplasm. The blue dashed lines represent nuclear membranes, and the red dashed lines represent cell membranes. Scale bars represent 1 μm.

The data are presented as the mean ± SEM. **$p < 0.01$, ***$p < 0.001$. See also Table S1 and Figures S1 and S14.

activity of GS (Zois and Harris, 2016). Here, we found that the activity of PhK was decreased at 12 h after reoxygenation following OGD (Figure 3I). The activity of PKA was also reduced during reoxygenation (Figure 3J). There was no change in the activity of GSK3α, an isoform of GSK3 (Figure 3K), but the activity of GSK3β was upregulated (Figure 3L).

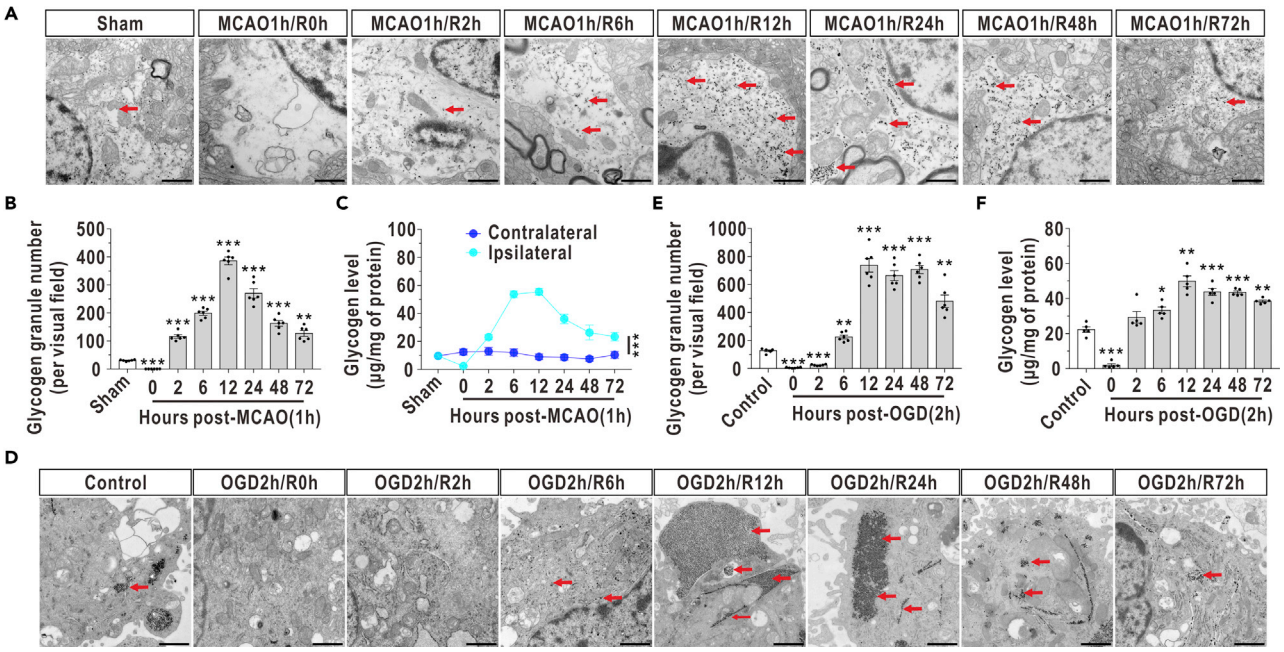

Figure 2. Glycogen Accumulation Lasts for at Least 72 h after I/R in Rodents and Cultured Astrocytes

(A) Representative electron microscopy images of brain glycogen in mice subjected to MCAO/R. The arrows indicate glycogen granules. Scale bars represent 1 μm.

(B and C) Quantified glycogen granules (B, n = 6, one-way ANOVA with the Dunnett T3 multiple comparisons test) and glycogen levels (C, n = 6, factorial analysis) in the ischemic penumbra after reperfusion.

(D) Representative electron microscopy images of glycogen in cultured astrocytes during reoxygenation. The arrows indicate glycogen granules. Scale bars represent 1 μm.

(E and F) Quantified glycogen granules (E, n = 6, one-way ANOVA with the Dunnett T3 multiple comparisons test) and glycogen levels (F, n = 5, one-way ANOVA with the Dunnett T3 multiple comparisons test) in cultured astrocytes after reoxygenation.

The data are presented as the mean ± SEM. *p < 0.05, **p < 0.01, ***p < 0.001.

Given that cultured astrocytes are unlikely to completely represent the *in vivo* situation, we adopted double-labeled immunofluorescence to specifically quantify the relative expressions of key enzymes in astrocytes in a mouse model of MCAO. First, the fluorescence intensity of S100β, used as an astrocytic marker in immunofluorescence, remained stable at 12 h after reperfusion (Figure S3). Second, we found that the expression of GS, GBE1, PYGM, PYGL, and AGL was relatively stable at 12 h after reperfusion in astrocytes (marked by S100β, Figures 4A, 4B, and 4D–4F). However, a 53.5% reduction in PYGB expression was observed at 12 h after MCAO/R (Figure 4C). Previous studies suggested that phosphorylated GS and N-terminal serine phosphorylated GSK-3β were the inactivated forms and that phosphorylation is the activated form for GP and PKA (Taylor et al., 2012; Wang et al., 2014; Zois and Harris, 2016). We found that the level of phosphorylated GS in astrocytes was not changed after reperfusion (Figure 4G). We also synthesized a new antibody against phosphorylated PYGB (Figure S4) and found that the level of phosphorylated PYGB in astrocytes dropped to 5.1% of that in the sham group at 12 h after MCAO/R (Figure 4H). In addition, we found that the level of phosphorylated PKA was significantly decreased at 12 h after reperfusion (Figure 4I) and that there was a decrease in the expression of inactivated phosphorylated GSK3β at 12 h after recanalization (Figure 4J).

Augmenting Astrocytic PYGB Increases the Survival of Both Astrocytes and Cocultured Neurons and Improves Neurological Outcomes after I/R

To determine the potential clinical significance of glycogen disorders in cerebrovascular disease, we first used lentiviruses to construct PYGB overexpression (Ve-Pygb) and CRISPR/Cas9-mediated PYGB knockdown (Sg-Pygb) models *in vitro* (Figure S5). We found that GP mRNA expression and *in vitro* activity were partially restored at 12 h after OGD/R in PYGB-overexpressing astrocytes, whereas PYGB knockdown reduced GP mRNA level and *in vitro* activity (Figures 5A and 5B). Elevated glycogen was decreased in the

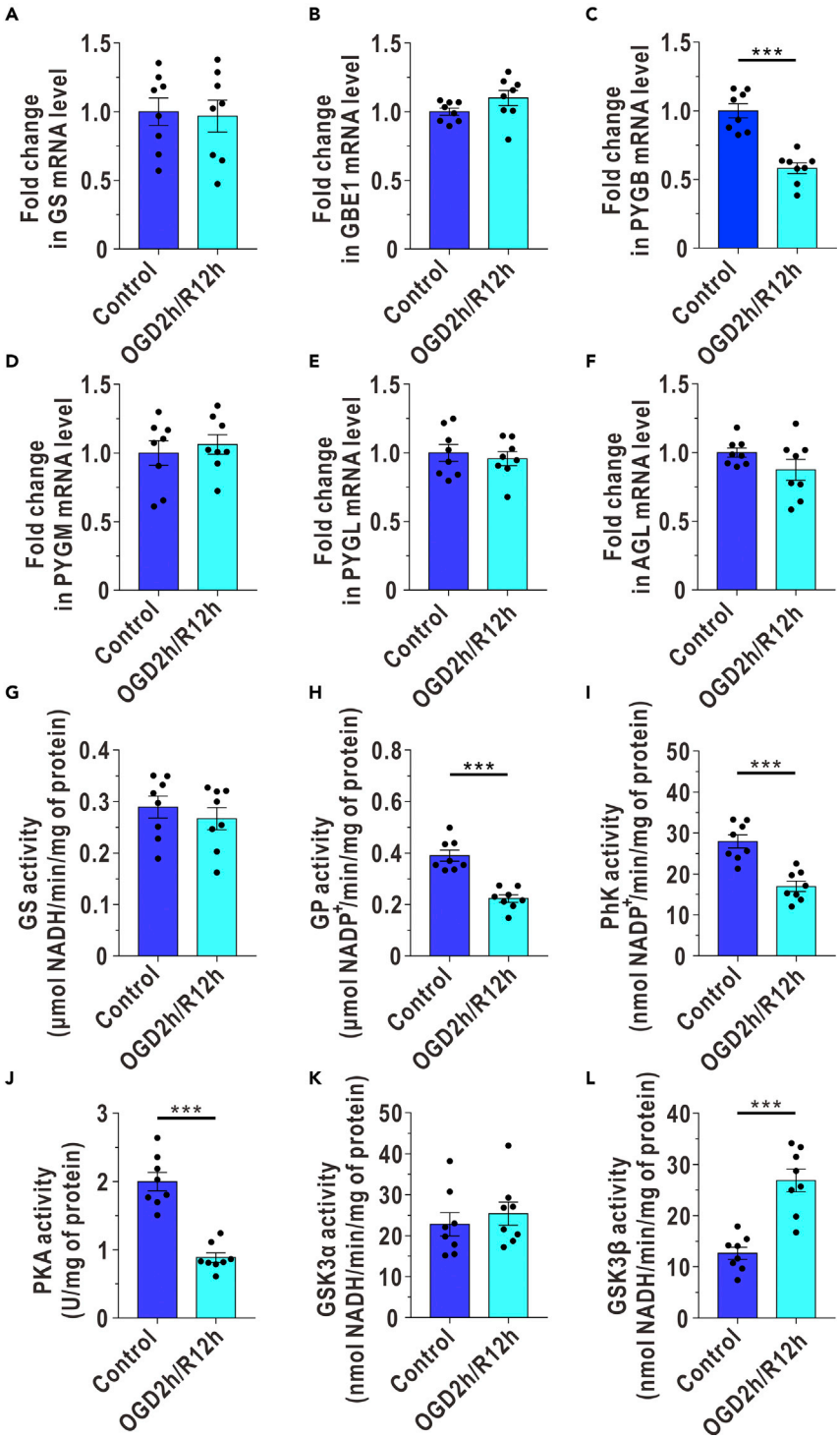

Figure 3. Relative mRNA Expressions and *In Vitro* Activities of Enzymes Involved in Glycogen Metabolism Are Selectively Reduced at 12 h after OGD/R in Cultured Astrocytes

(A–F) The mRNA levels of GS (A), GBE1 (B), PYGB (C), PYGM (D), PYGL (E), and AGL (F) were determined by quantitative reverse transcription polymerase chain reaction (RT-qPCR) at 12 h after reoxygenation in cultured astrocytes (n = 8, independent t test).

(G–L) Quantified GS (G), GP (H), PhK (I), PKA (J), GSK3α (K), and GSK3β (L) activities in astrocytes at 12 h after reoxygenation in cultured astrocytes (n = 8, independent t test).

The data are presented as the mean ± SEM. ***p < 0.001. See also Figure S2 and Table S3.

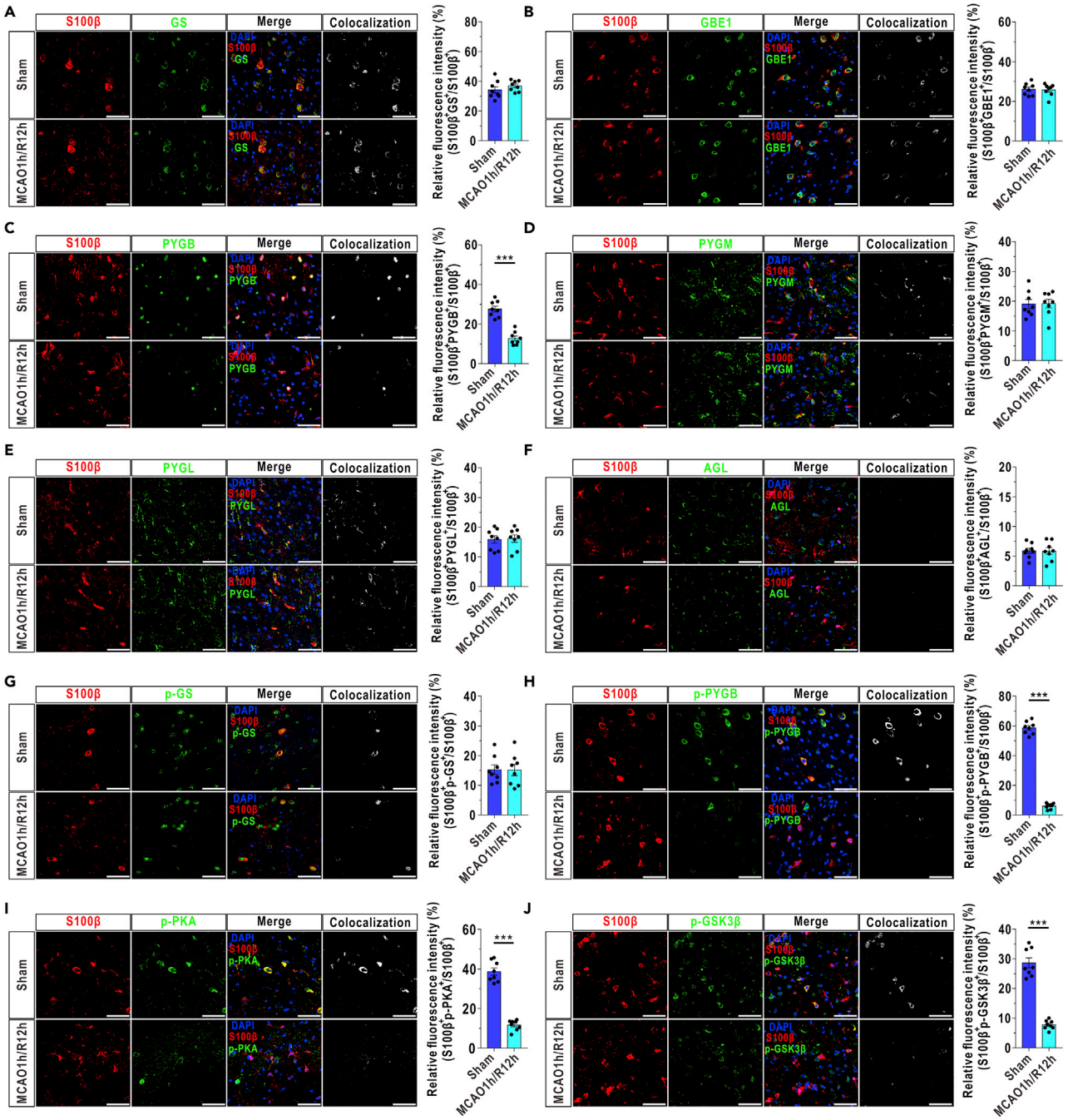

Figure 4. Protein Levels of Enzymes Involved in Glycogen Metabolism Are Selectively Reduced after Reperfusion in a Mouse Stroke Model

(A–F) Left panels: coronal immunofluorescence images of frontal cortex area 1 in the ischemic penumbra after staining with an antibody against S100β and antibodies against GS (A), GBE1 (B), PYGB (C), PYGM (D), PYGL (E), and AGL (F). Right panels: quantification of relative fluorescence intensity of GS (A), GBE1 (B), PYGB (C), PYGM (D), PYGL (E), and AGL (F) in astrocytes of the ischemic penumbra at 12 h after reperfusion (n = 8, independent t test). Astrocytes were marked with S100β. The relative fluorescence intensity of the target protein was calculated as the percentage of fluorescence intensity in the colocalization area (denoted as S100β and target protein) divided by the fluorescence intensity in the $S100\beta^+$ area. Scale bars represent 50 μm.

(G–J) Left panels: coronal immunofluorescence images of frontal cortex area 1 in the ischemic penumbra after staining with an antibody against S100β and antibodies against phosphorylated GS (p-GS, G), phosphorylated PYGB (p-PYGB, H), phosphorylated PKA (p-PKA, I) and phosphorylated GSK3β (p-GSK3β, J). Right panels: quantification of relative fluorescence intensity of p-GS (G), p-PYGB (H), p-PKA (I), and p-GSK3β (J) in astrocytes of the ischemic penumbra at 12 h after reperfusion (n = 8, independent ttest). Astrocytes were marked with S100β. Scale bars represent 50 μm.

The data are presented as the mean ± SEM. ***$p < 0.001$. See also Figure S3, S4, and S13 and Table S2.

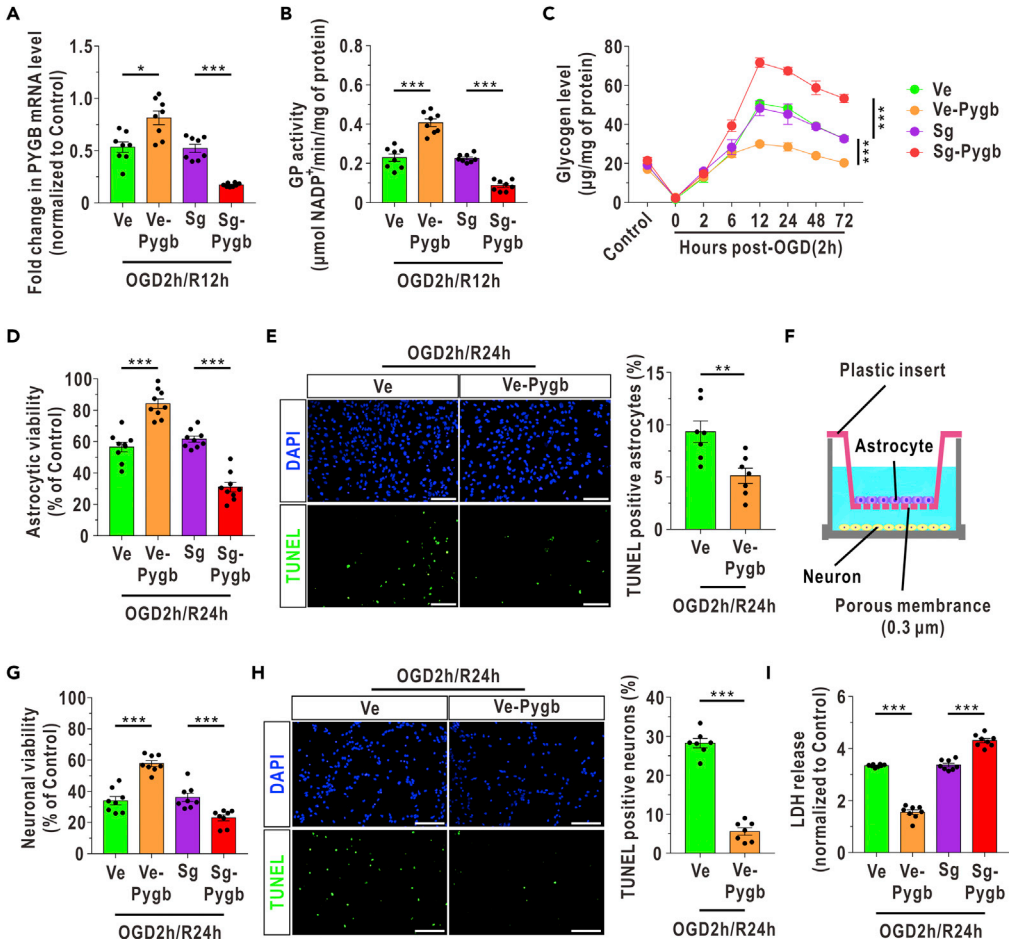

Figure 5. Enhancement of Astrocytic PYGB Improves the Survival of Cultured Astrocytes and Cocultured Neurons During OGD/R

(A) Quantified PYGB mRNA levels in PYGB-overexpressing (Ve-Pygb) and PYGB-knockdown (Sg-Pygb) cultured astrocytes at 12 h after reoxygenation (n = 8, one-way ANOVA with the Dunnett T3 multiple comparisons test). Sg represents astrocytes infected with scrambled sgRNA lentiviruses. Ve represents astrocytes infected with blank vector lentiviruses.

(B) Quantified GP activity in PYGB overexpressing and knockdown cultured astrocytes at 12 h after reoxygenation (n = 8, one-way ANOVA with the Dunnett T3 multiple comparisons test).

(C) Glycogen concentrations in PYGB overexpressing and knockdown cultured astrocytes during OGD/R stress (n = 3, factorial analysis).

(D) The relative cell viability of cultured astrocytes was determined by a Cell Counting Kit-8 (CCK-8) assay at 24 h after the onset of reoxygenation (n = 9, one-way ANOVA with the LSD multiple comparisons test). The control condition means that the astrocytes received only culture medium changes (containing glucose) at the same timepoints as the OGD/R group but no OGD stress.

(E) The numbers of apoptotic cultured astrocytes at 24 h after OGD/R were analyzed by TUNEL staining (n = 7, independent t test). The top panel represents the total cells stained by DAPI, and the bottom panel represents the apoptotic astrocytes stained by TUNEL. Scale bars represent 100 μm.

(F) Diagram of the astrocyte-neuron coculture system.

(G) Viability of neurons at 24 h after reoxygenation in the coculture system (n = 8, one-way ANOVA with the LSD multiple comparisons test). The control condition means that the cocultured neurons received only culture medium changes (containing glucose) at the same timepoints as the OGD/R group but no OGD stress.

(H) Apoptosis analysis of neurons at 24 h after reoxygenation in the coculture system (n = 7, independent t test). Scale bars represent 100 μm.

(I) LDH release in the coculture medium (n = 8, one-way ANOVA with the Dunnett T3 multiple comparisons test).

The data are presented as the mean ± SEM. *p < 0.05, **p < 0.01, ***p < 0.001. See also Figure S5, S6, and S15 and Table S3.

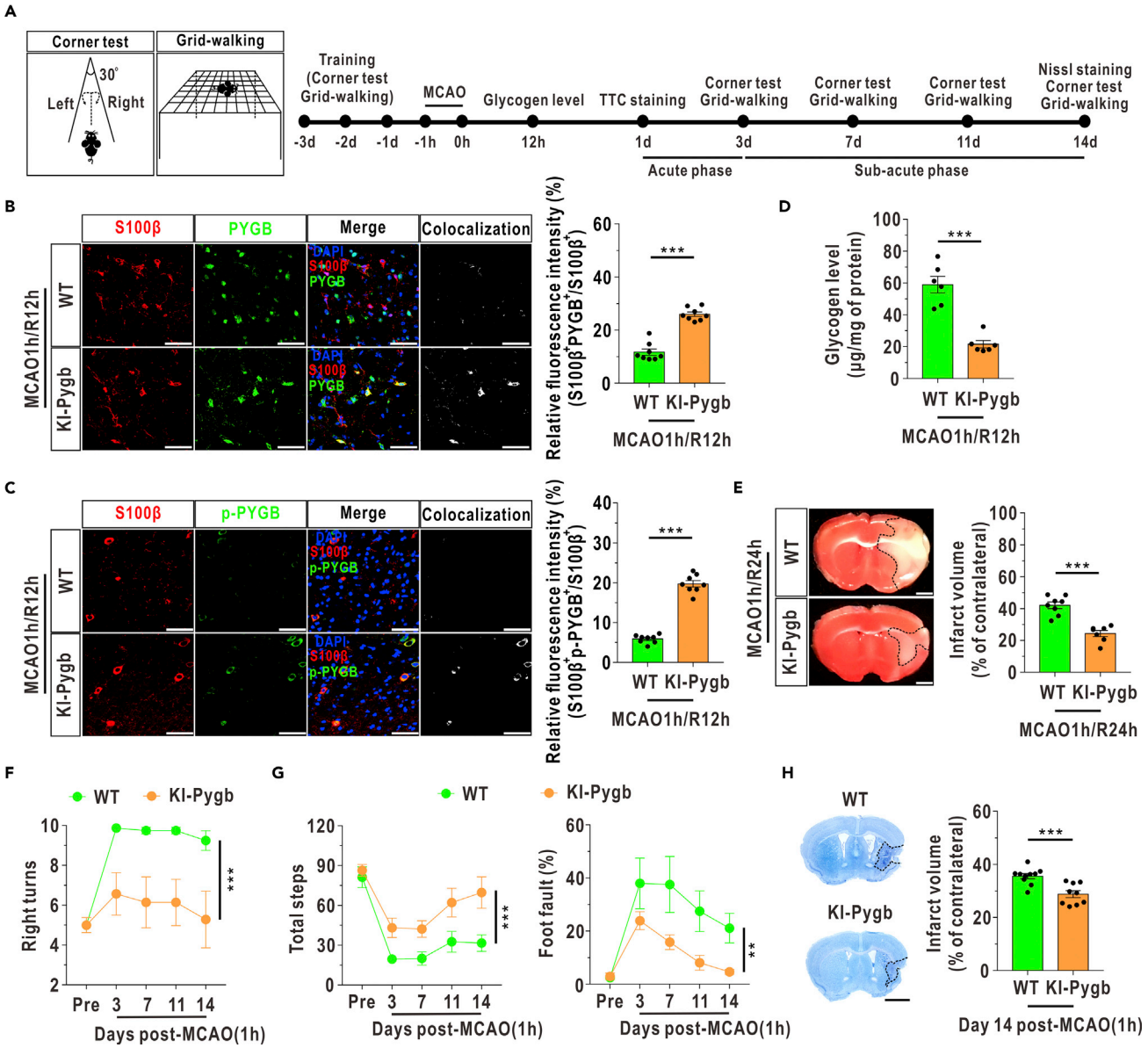

Figure 6. Enhancement of Astrocytic PYGB Ameliorates Ischemic Outcomes during MCAO/R

(A) Left panel: schematic of the corner test and grid-walking test patterns. Right panel: timeline of biochemical, neurobehavioral, and neuropathological analyses after MCAO/R treatment.

(B) Left panel: coronal immunofluorescence images of frontal cortex area 1 in the ischemic penumbra after staining with an antibody against S100β and an antibody against PYGB. Right panel: quantification of relative fluorescence intensity of PYGB in astrocyte-specific PYGB knock-in (KI-Pygb) mice and WT mice at 12 h after reperfusion (n = 8, independent t test). Astrocytes were marked with S100β. The relative fluorescence intensity of PYGB was calculated as the percentage of fluorescence intensity in the colocalization area (denoted as S100β and PYGB) divided by the fluorescence intensity in the $S100\beta^+$ area. Scale bars represent 50 μm.

(C) Left panel: coronal immunofluorescence images of frontal cortex area 1 in the ischemic penumbra after staining with an antibody against S100β and an antibody against phosphorylated PYGB (p-PYGB). Right panel: quantification of relative fluorescence intensity of p-PYGB in KI-Pygb mice and WT mice at 12 h after reperfusion (n = 8, independent t test). Astrocytes were marked with S100β. Scale bars represent 50 μm.

(D) Cerebral glycogen levels in the ischemic penumbra at 12 h after MCAO/R (n = 6, independent t test).

(E) Left panel: representative brain slice images of triphenyltetrazolium chloride (TTC) staining at 24 h after MCAO/R. Right panel: the quantified infarct volumes of TTC staining (WT: n = 8; KI-Pygb: n = 7, independent ttest). Scale bars represent 1 mm.

(F) A corner test was performed to analyze the numbers of right turns in 10 trials before (Pre) and after reperfusion in the mouse model of MCAO (WT: n = 8; KI-Pygb: n = 7, repeated measures analysis).

Figure 6. *Continued*

(G) A grid-walking test was performed to assess the total steps (left panel) and foot fault ratios (right panel) before (Pre) and after reperfusion in the mouse model of MCAO (WT: n = 8; KI-Pygb: n = 7, repeated measures analysis).

(H) Nissl staining was used to assess infarct volumes at day 14 after MCAO/R (WT: n = 10; KI-Pygb: n = 9, independent ttest). Scale bar represents 2 mm. The data are presented as the mean ± SEM. **p < 0.01. ***p < 0.001. See also Figure S7 and Video S1 and Table S2.

PYGB overexpression model but was further increased with PYGB knockdown after OGD/R (Figure 5C). Next, the cell viability of astrocytes increased with PYGB overexpression and decreased with PYGB knockdown under OGD/R insult (Figure 5D). The proportion of apoptotic astrocytes also decreased with PYGB overexpression (Figure 5E). In addition, we found that a pharmacological PKA agonist (8-Br-cAMP, 10 μM) significantly activated GP and suppressed GS at 12 h after OGD/R (Figures S6A and S6B). Glycogen levels also decreased and the viability of astrocytes increased upon treatment with 8-Br-cAMP (Figures S6C and S6D).

Considering the metabolic coupling between astrocytes and neurons, a coculture system was used that allowed the two cell types to share diffusible metabolic substrates but remain divided by a physical filter (Figure 5F). After genetic enhancement of astrocytic PYGB, the viability of neurons was significantly increased, whereas the number of apoptotic neurons was markedly decreased during reoxygenation (Figures 5G and 5H). In contrast, neuronal viability decreased when astrocytic PYGB was silenced (Figure 5G). The observed decreases in lactate dehydrogenase (LDH) in the coculture medium further revealed that the overall survival of neurons and astrocytes was promoted by the augmentation of astrocytic PYGB during OGD/R (Figure 5I).

To evaluate whether genetic enhancement of astrocyticglycogenolysis alleviates brain injury, a knock-in mouse model with astrocyte-specific PYGB overexpression (KI-Pygb) was constructed, and the KI-Pygb mice showed no differences in appearance but had increases in the expressions of PYGB and phosphorylated PYGB compared with those of their wild-type (WT) littermate controls (Figure S7). Histological and neurobehavioral analyses were performed in the acute and subacute phases (Mullins, 2006) after MCAO/R, according to the timeline shown in Figure 6A. Immunofluorescence analysis revealed that the expression of PYGB and phosphorylated PYGB in astrocytes was partially restored at 12 h after reperfusion in transgenic mice compared with WT mice (Figures 6B and 6C). Accordingly, brain glycogen accumulation was significantly attenuated at 12 h after reperfusion in KI-Pygb mice compared with WT mice (Figure 6D). The infarct volumes were notably decreased in KI-Pygb mice during the acute phase after reperfusion (Figure 6E). In addition, a corner test was performed to assess sensorimotor dysfunction (Zhang et al., 2002), and the number of right turns was clearly decreased in the KI-Pygb mice compared with the WT group after reperfusion (Figure 6F). A grid-walking test was also performed to detect the degree of motor impairment (Barbosa et al., 2016), and PYGB enhancement led to significant increases in total steps and decreases in the foot fault ratio after restoration of circulation (Video S1 and Figure 6G). The infarct volumes were markedly decreased in the KI-Pygb mice during the subacute phase after MCAO/R, as revealed by Nissl staining (Figure 6H).

Insulin Mediates Neuroprotection by Rebalancing Glycogen Metabolism via Activation of PKA/PhK and Suppression of GSK-3β

Insulin is a proteohormone that is critical for the maintenance of hepatic glycogen homeostasis (Moore et al., 2012) and mediates cardioprotective effects on I/R in heart (Bertrand et al., 2008). Here, we found that the increased glycogen levels gradually returned to normal levels after treatment with increasing concentrations of insulin (IS) during reoxygenation (Figure 7A). In addition, a significant increase in GP activity, but no effect on GS activity, was found in cultured astrocytes at 12 h after OGD/R with insulin (1 μM) treatment (Figures 7B, 7C, and S8). Unexpectedly, insulin was observed to enhance GS activity rather than GP activity in normal cultured astrocytes (Figure S9). This discrepancy prompted us to uncover the upstream alterations in glycogen metabolism. We found that both PhK and PKA were upregulated at 12 h after reoxygenation after insulin treatment (Figures 7D and 7E). The activity of GSK3β was decreased with insulin treatment, whereas the activity of GSK3α was unchanged (Figures 7F and 7G). Subsequently, similar to the above data *in vitro*, intracerebroventricular insulin (10 μM) treatment increased the levels of phosphorylated PYGB, PKA, and GSK3β, with no effects on phosphorylated GS in mouse brains at 12 h after blood recirculation (Figures 7H–7K). And the fluorescence intensity of S100β remained stable with intracerebroventricular insulin treatment for 12 h (Figure S10).

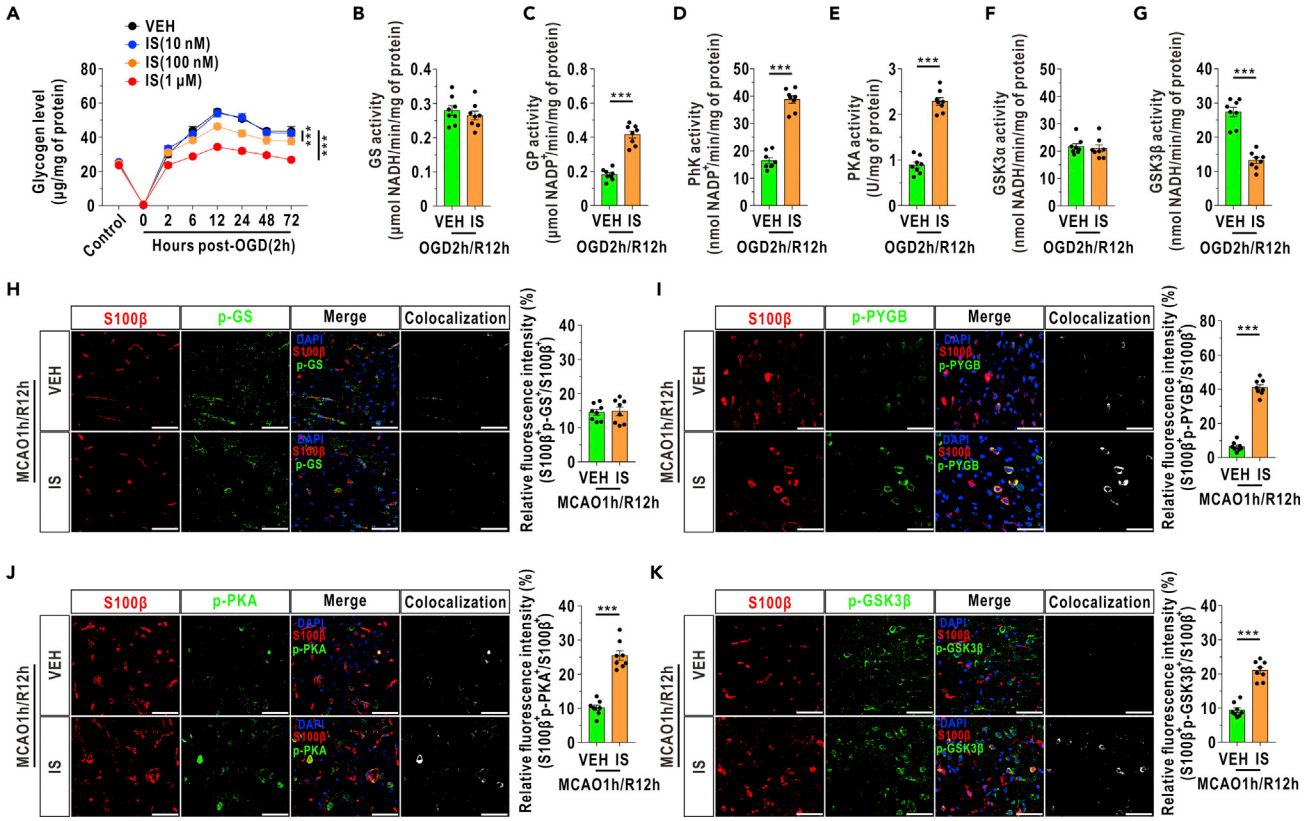

Figure 7. Insulin Activates GP, PhK, and PKA Activities and Suppresses GSK3β Activity in Cultured Astrocytes and Increases Their Relative Fluorescence in Rodents after I/R

(A) Glycogen concentrations in cultured astrocytes treated with different doses of insulin after reoxygenation (n = 4, factorial analysis). Insulin was added to the medium immediately after reoxygenation. VEH represents the vehicle group, and IS represents the insulin group.

(B–G) The activities of GS (B), GP (C), PhK (D), PKA (E), GSK3α (F), and GSK3β (G) were quantified at 12 h after reoxygenation in cultured astrocytes treated with insulin (1 μM) (n = 8, independent t test).

(H–K) Left panels: coronal immunofluorescence images of frontal cortex area 1 in the ischemic penumbra after staining with an antibody against S100β and antibodies against phosphorylated GS (p-GS, H), phosphorylated PYGB (p-PYGB, I), phosphorylated PKA (p-PKA, J), and phosphorylated GSK3β (p-GSK3β, K). Right panels: quantification of relative fluorescence intensity of p-GS (H), p-PYGB (I), p-PKA (J), and p-GSK3β (K) in the ischemic penumbra at 12 h after reperfusion (n = 8, independent t test). Astrocytes were marked with S100β. Insulin (10 μM) was injected into the lateral ventricle immediately after reperfusion to achieve a final concentration of approximately 1 μM in the cerebrospinal fluid. The relative fluorescence intensity of the target protein was calculated as the percentage of fluorescence intensity in the colocalization area (denoted as S100β and target protein) divided by the fluorescence intensity in the $S100\beta^+$ area. Scale bars represent 50 μm.

The data are presented as the mean ± SEM. ***p < 0.001. See also Figures S8–S10 and Table S2.

We next examined the role of astrocyticglycogenolysis in insulin-mediated neuroprotection using Sg-Pygb models *in vitro*. The insulin-induced decrease in glycogen was attenuated in GP knockdown astrocytes during OGD/R (Figure 8A). Astrocyte survival appeared to be increased with insulin treatment but decreased with concomitant PYGB knockdown lentivirus treatment during reoxygenation, as determined by cell viability and apoptosis rate analyses (Figures 8B and 8C). Cocultured neuron survival was notably improved by insulin treatment during OGD/R, and this improvement could be blocked by coculture with GP knockdown astrocytes (Figures 8D and 8E). LDH release into the coculture medium also decreased with insulin treatment and increased when astrocytic PYGB was inhibited during reoxygenation (Figure 8F).

To conditionally suppress astrocytic PYGB expression *in vivo*, an adeno-associated virus (AAV) containing the astrocyte-specific glial fibrillary acidic protein (GFAP) promoter (Brenner et al., 1994) and an exogenous short hairpin RNA (shRNA) targeting the *pgyb* gene was constructed (Sh-Pygb). Exogenous shRNA, which was marked by FLAG, was predominantly localized in astrocytes, which were marked by GFAP (Figure S11A). The expression of astrocytic PYGB and phosphorylated PYGB was clearly downregulated in the PYGB knockdown mice (Figures S11B–S11D). The accumulated glycogen in the mouse brain was

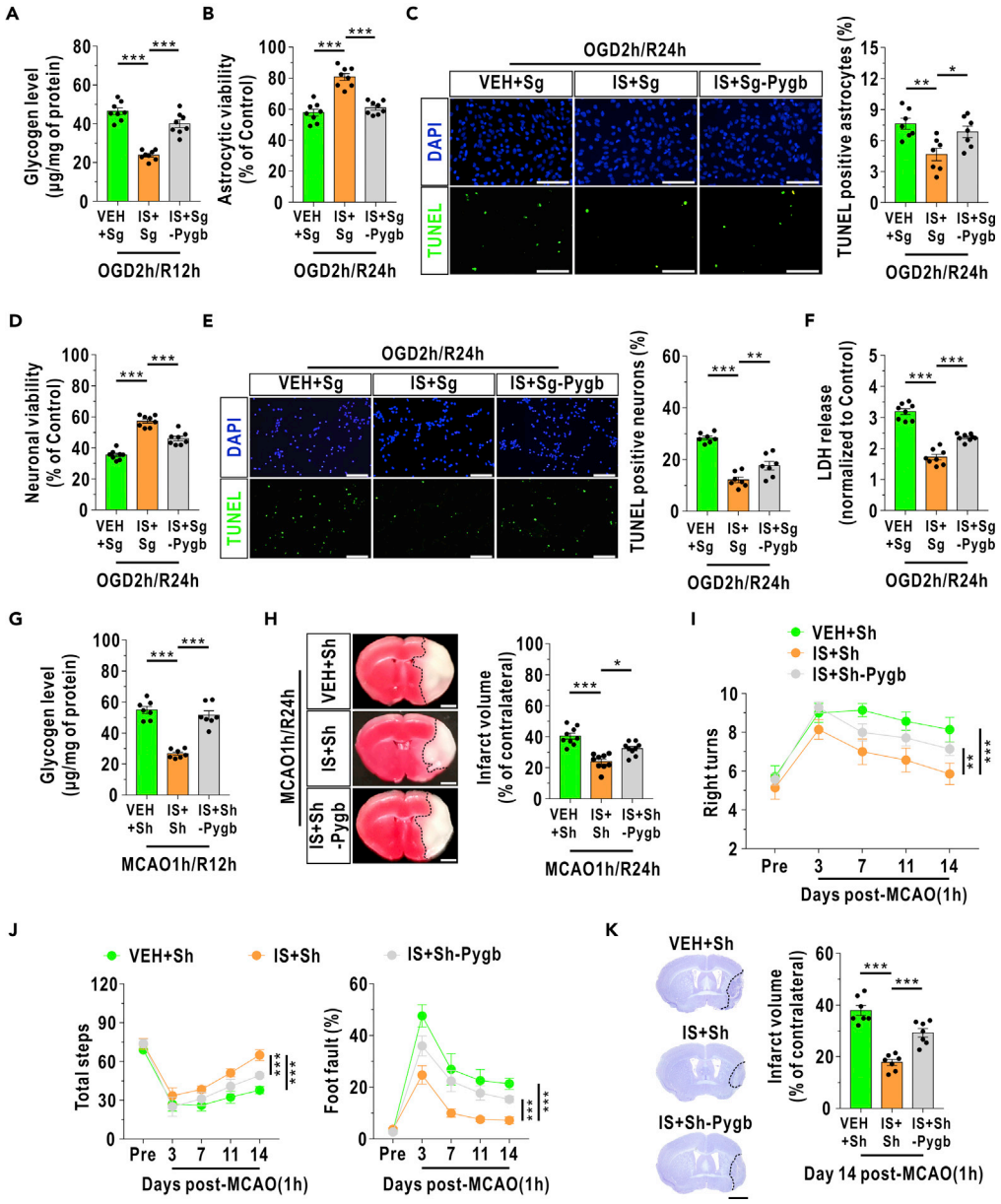

Figure 8. Insulin Decreases Astrocyte and Neuron Death and Protects the Brain Damage during I/R Injury by Enhancing Astrocytic GP Activity

(A) Glycogen level in cultured astrocytes at 12 h after OGD/R (n = 8, one-way ANOVA with the LSD multiple comparisons test). Insulin (1 μM) was added to the medium immediately after reoxygenation. VEH represents the vehicle group, and IS represents the insulin group. Sg represents astrocytes infected with scrambled sgRNA lentiviruses. Sg-Pygb represents GP-knockdown astrocytes.

(B) Relative cell viability of the cultured astrocytes at 24 h after reoxygenation (n = 8, one-way ANOVA with the LSD multiple comparisons test). The control condition means that the astrocytes received culture medium changes (containing glucose) without OGD/R stress.

(C) The numbers of apoptotic cultured astrocytes were analyzed by TUNEL staining at 24 h after reoxygenation (n = 7, one-way ANOVA with the LSD multiple comparisons test). Scale bars represent 100 μm.

(D) Viability of neurons treated at 24 h after reoxygenation in the astrocyte-neuron coculture system (n = 8, one-way ANOVA with the LSD multiple comparisons test). The control condition means that the cocultured neurons received culture medium changes (containing glucose) without OGD/R stress.

(E) The numbers of apoptotic neurons in coculture were analyzed by TUNEL staining at 24 h after reoxygenation (n = 7, one-way ANOVA with the LSD multiple comparisons test). Scale bars represent 100 μm.

Figure 8. *Continued*

(F) LDH release in the coculture medium was analyzed (n = 8, one-way ANOVA with the Dunnett T3 multiple comparisons test).

(G) Glycogen levels in the ischemic penumbra at 12 h after MCAO/R in mice (n = 7, one-way ANOVA with the LSD multiple comparisons test). Insulin (10 μM) was injected into the lateral ventricle immediately after reperfusion to achieve a final concentration of approximately 1 μM in the cerebrospinal fluid. Sh represents mice infected with scrambled shRNA AAVs. Sh-Pygb represents PYGB knockdown mice.

(H) The infarct volumes at 24 h after MCAO/R in mice were analyzed by TTC staining (n = 9, one-way ANOVA with the LSD multiple comparisons test). Scale bars represent 1 mm.

(I) A corner test was performed to analyze the numbers of right turns in 10 trials before (Pre) and after reperfusion in the mouse model of MCAO (n = 7, repeated measures analysis).

(J) A grid-walking test was performed to assess the total steps (left panel) and foot fault ratios (right panel) before (Pre) and after reperfusion in the mouse model of MCAO (n = 7, repeated measures analysis).

(K) Nissl staining was used to assess infarct volumes at day 14 after MCAO/R in mice (n = 7, one-way ANOVA with the LSD multiple comparisons test). Scale bar represents 2 mm.

The data are presented as the mean ± SEM. *p < 0.05, **p < 0.01, ***p < 0.001. See also Figures S11 and S12.

also diminished with insulin treatment after reperfusion, and the decreases in glycogen were suppressed in mice with *pygb*-modified astrocytes (Figure 8G). Furthermore, the infarct volumes were decreased after insulin administration, and astrocytic PYGB inhibition blocked this effect at 24 h after MCAO/R (Figure 8H). Consistent with the above acute-phase data, neurobehavioral and neuropathological impairments were revealed to be significantly alleviated with insulin treatment in the corner test (Figure 8I) and grid-walking test (Figure 8J) and by Nissl staining (Figure 8K) during the subacute phase of recirculation; these effects were markedly blocked when astrocyticglycogenolysis was suppressed. In addition, intraventricular injection of insulin did not affect blood glucose after MCAO/R operation (Figure S12).

DISCUSSION

The present study reveals that the accumulation of glycogen is strongly associated with the development of I/R injury in mice subjected to transient cerebral ischemia and cultured astrocytes treated with OGD. Our findings provide the evidence that glycogen accumulation is common across species following transient cerebral ischemia. We found that PYGB, the brain isoform of GP in glycogenolysis, plays a substantial role in glycogen-accumulation-associated neuropathy. The PKA-PhK-GP cascade participates in the reprogramming of glycogenolysis during recanalization after ischemic stroke and reoxygenation after OGD.

In this study, we examined cerebral glycogen levels after stroke in humans and nonhuman primates and found that glycogen was excessively accumulated in the ischemic penumbra of humans and nonhuman primates after cerebral I/R, which is consistent with findings from previous observations in rodents (Folbergrova et al., 1996; Gurer et al., 2009; Hossain et al., 2014; Kajihara et al., 2001). To determine the time window for glycogen accumulation after cerebral I/R, brain glycogen levels were continuously detected until 72 h after reperfusion in a focal ischemia rodent model, and we showed that astrocytic glycogen accumulated at 6 h and peaked at 12 h after cerebral reperfusion. Notably, postmortem tissue handling caused glycogen loss in the contralateral hemisphere of stroke patients in this study, because glycogen levels in Figure 1A were reduced to approximately 13% compared with those reported in a previous study (Kirsch and Leitner, 1967). Postmortem loss of glycogen could also be expected in the monkey and mouse brains and cultured astrocytes due to the lag time between decapitation and freezing or cell lysis (See Transparent Methods).

Considering the pivotal role of glycogen in maintaining cerebral physiological function, elucidation of the underlying mechanism of reperfusion-induced glycogen accumulation is necessary. Limited evidence suggests that GSK3beta activity is upregulated during I/R stress (Ramagiri and Taliyan, 2017). Theoretically, GSK3β inhibits GS activity through phosphorylation, and inactivation of GS could decrease the levels of glycogen during I/R (Pederson, 2019). However, where is the excessive glycogen in astrocytes derived from after recirculation? The PKA-PhK-GP pathway has been revealed to determine glycogen degradation in the liver, and PKA can suppress GS activity as well (Zois and Harris, 2016). These clues prompted us to investigate the alterations of these key enzymes in glycogen metabolism. We found that the astrocytic PKA-PhK-GP cascade was significantly inactivated during reperfusion. The activity of GS remained at normal levels due to the neutralizing effects of PKA suppression and GSK3β activation. Interestingly, inequality of changes in mRNA level and protein level related to enzyme activity was found in this study. For instance, Figure 4C showed a 53.5% reduction in PYGB expression, whereas the level of phosphorylated PYGB in astrocytes dropped to 5.1% at 12 h after MCAO/R in Figure 4H. Also, in Figure 7C, the

in vitro activity of GP increased after insulin-treated, whereas its protein level was still decreased at 12 h after OGD/R (Figure S8C). In addition, we observed that the expression of PYGB was preferentially affected in mice suffered from MCAO/R and in cultured astrocytes subjected to OGD/R compared with that of PYGM and PYGL. We are not sure whether only PYGB activity was also decreased during reperfusion because the activities of PYGM and PYGL were not detected in this study. No evidence suggests that the PKA-PhK pathway regulates only PYGB not PYGM or PYGL activity. Therefore, we speculate that PYGB is vulnerable to I/R mainly because it accounts for a large proportion of GP mRNA isoforms in cultured astrocytes (91.7%).

Our findings seem to be inconsistent with the existing idea that glycogen storage caused by pharmacological inhibition of glycogenolysis can prevent energy crisis and alleviate brain damage. Constant perfusion of the glycogen breakdown inhibitor, ingliforib, to increase glycogen levels 30 min before myocardial ischemia shows a cardioprotective effect, because glycogen is rapidly degraded to glucose-1-phosphate to provide additional energy (Tracey et al., 2004). Some GP inhibitors, such as CP-316819 and maslinic acid, have also been used to elevate the levels of brain glycogen before brain ischemia (Guan et al., 2011; Xu and Sun, 2010). Release of prestored glycogen has been viewed as a promising therapeutic strategy to rapidly supply energy under ischemia and alleviate brain damage (Xu and Sun, 2010). However, pharmacological treatments targeting glycogenolysis should be carefully used. Our results showed that reprogramming of GP and impairment of glycogen breakdown, instead of glycogen deficit, occurred during the reperfusion phase. Previous studies also revealed that the elevation of glycogen levels during recirculation is prolonged in proportion to the duration of ischemia (Long et al., 1972; Mrsulja et al., 1975, 1979). We strongly suspect that sustained pharmacological action of these GP inhibitors during the reperfusion stage will lead to an aggravated ischemic outcome. Therefore, the timing of pharmacological intervention is particularly important, and short-acting GP antagonists and GP agonists may need be administered separately before ischemia and after reperfusion, respectively, according to the patient's condition.

In this study, we revealed that the mobilization of glycogenolysis in astrocytes contributes to the survival of neighboring neurons after reperfusion. This phenomenon is interesting, but the underlying mechanism might be complicated. Previous studies have provided clues about how degraded glycogen attenuates neuronal damage. First, extra glycogen could fuel Na^+/K^+-ATPase to enhance K^+ uptake in astrocytes and improve neuronal excitation recovery (Xu et al., 2013). The activation of Na^+/K^+-ATPase also accelerates excitatory glutamate uptake by stimulating the excitatory amino acid transporter and attenuates glutamate excitotoxicity to neurons (Xu et al., 2014; Yin et al., 2019). In addition, glycogen might provide energy for loading Ca^{2+} into the ER and relieve the neuronal damage caused by calcium overload (Müller et al., 2014). Finally, increased glucose-6-phosphate resulting from glycogen feedback inhibits hexokinase, thereby reducing astrocyte consumption of blood-borne glucose and sparing glucose in neurons (Dienel and Rothman, 2019). Notably, we observed a 43% reduction in glycolytic capacity during OGD/R stress in this study. However, this did not confirm that degraded glycogen could not be used as a fuel for astrocytes because the capacity of most enzymes is suggested to greatly exceed the flux through the metabolic step (Lowry and Passonneau, 1964). In a word, we speculate that in the context of ischemia, compromised astrocytes can boost their energy reserves by reprogramming astrocyte-neuron interactions after reperfusion. Further study should focus on these pathways to elucidate the underlying metabolic profiles during glycogen mobilization and to determine their implications for clinical stroke therapy.

During the past several decades, the glucose, insulin, and potassium (GIK) metabolic cocktail has been widely used in the clinic for cardioprotection after myocardial infarction. Growing evidence has revealed that insulin, but not glucose or potassium, plays an important role in the protective effects of GIK against I/R injury (Zhang et al., 2006). The underlying mechanism of insulin-mediated neuroprotection has been reported to primarily depend on maintenance of calcium homeostasis, inhibition of inflammation, and down-regulation of free radical release in heart (Bertrand et al., 2008). In addition, insulin can stimulate erythropoietin production (Masuda et al., 1997), regulate gliotransmission (Cai et al., 2018), and modulate glucose metabolism (Fernandez et al., 2017) in astrocytes and stimulate glucose utilization (Ashrafi et al., 2017; Pearson-Leary et al., 2018) in neurons, which may also contribute to recovery after I/R. However, we cannot ignore the fact that insulin is an important regulator of glycogen homeostasis in the body and that its glycogenic target in the context of neuroprotection is far from completely understood. Recent studies revealed that insulin suppresses the activity of GSK3β through activation of the phosphatidylinositol 3-kinase (PI3K)-protein kinase B (PKB) pathway upon I/R stress (Bertrand et al., 2008; Mishra et al., 2018). Notably, the

levels of brain glycogen decreased with insulin treatment during reperfusion in this study, which seems to contradict the finding that insulin promotes glycogen synthesis by inhibiting GSK3β. Here, we found that insulin could also activate the PKA-PhK-GP pathway and that the neuroprotective effects of insulin could be attenuated by PYGB knockdown, which may account for the contribution of insulin-mediated recovery during the acute and subacute phases after stroke. Therefore, insulin in the brain is more likely to act as a coordinator to maintain glycogen metabolic homeostasis rather than to simply accelerate glycogen synthesis when the level of glycogen has already substantially increased during reperfusion.

Collectively, our findings provide evidence that glycogen accumulation occurs in humans and monkeys following transient ischemia and that reprogramming of glycogenolysis leads to astrocytic glycogen accumulation and brain damage. Enhancing glycogenolytic metabolism during the acute stage of reperfusion may protect the brain from I/R injury. These results also support the notion that the activated PKA-PhK-GP cascade underlies insulin-mediated neuroprotection. Thus, glycogenolysis is a potential intervention target for ischemic stroke, but the precise application of targeting strategies should be carefully considered according to the timing of ischemia.

Limitations of the Study

One limitation is the possibility that I/R insult has effects on malin or laforin, leading to an abnormal structure of glycogen that then accumulates, as in Lafora disease (Dukhande et al., 2011; Gentry et al., 2005), which is independent of deficits in GP and its upstream signaling pathways. In our study, we did not detect the activities of laforin and malin in I/R injury. However, we observed that cerebral reperfusion did not induce changes in the expression of laforin and malin in astrocytes (Figure S13). In addition, a previous study revealed that accumulated glycogen is not restricted to astrocytes but can be detected in neurons in Lafora disease (Augé et al., 2018). As shown in Figure 1C, no accumulated glycogen granules were found in neurons using electron microscopy in the mouse MCAO/R model. Therefore, it is conceivable that glycogen accumulation was not due to laforin or malin dysfunction during cerebral reperfusion disorders, but this remains to be further tested.

Another limitation is the existence of some methodological weaknesses in this study. First, the lag time of dissection to obtain the penumbra tissue in sample handling during the glycogen quantitative assay caused glycogen loss. Previous studies suggest that at least 50% of glycogen degrades in 30 s after decapitation in adult mice (Lowry et al., 1964), and our glycogen levels in the mouse cortex are approximately half of those reported previously (Oe et al., 2016). In addition, all methods to harvest tissue and cells for glycogen assays had a lag time before freezing or lysis during which glycogenolysis might have occurred, particularly in the control samples where GP activity was not affected. This would cause underestimation of glycogen concentration in the control samples and overestimation of relative postischemic concentration. Therefore, microwave fixation of mouse brain tissue, which preserves glycogen much better than decapitation (Oe et al., 2016), should be adopted for glycogen quantitative assays in future studies. Secondly, double-labeled immunofluorescence has some disadvantages for the quantification of enzyme activity *in vivo*. The S100β is mainly in astrocytic soma that reports only about 15% of the cell volume (Bushong et al., 2002), and most of the volume that also contains about half of the glycogen (Oe et al., 2016) and presumably related enzymes is actually in the small processes that were not analyzed in the present study. In addition, the expression of phosphorylated enzyme does not equal the actual activity of the enzyme, and the relationship between fluorescence intensity and expression of the target protein is not linear (Barnett et al., 2019; Odell and Cook, 2013), which illustrates that immunofluorescence is imprecise and only a semiquantitative method to evaluate enzyme activities *in vivo*. More precise methods might be developed to quantify astrocyte-specific enzyme activity *in vivo*. Thirdly, hyperglycemia is known to worsen stroke outcome (Zhang et al., 2013) and use of 25 mM glucose in the cultures might exaggerate damage caused by OGD in this study. Normal glucose medium (5.5 mM glucose) should be used in the future related studies.

Resource Availability

Lead Contact

Further information and requests for resources and reagents should be directed to and will be fulfilled by the Lead Contact, Lize Xiong (mzkxlz@126.com).

Materials Availability

Viruses and mouse lines generated in this study have been deposited in the laboratory of Department of Anesthesiology and Perioperative Medicine, Xijing Hospital, Fourth Military Medical University. Viruses and mouse lines generated in this study will be made available on request, but we may require a payment and a completed Materials Transfer Agreement if there is potential for commercial application.

Data and Code Availability

All relevant data are available from the corresponding author (L.X.) upon reasonable request. This study did not generate code.

METHODS

All methods can be found in the accompanying Transparent Methods supplemental file.

SUPPLEMENTAL INFORMATION

Supplemental Information can be found online at https://doi.org/10.1016/j.isci.2020.101136.

ACKNOWLEDGMENTS

This work was supported by funds from the Major Programs of the National Natural Science Foundation of China (No. 81590954), the International Cooperation and Exchange of the National Natural Science Foundation of China (No.81420108013), the National Natural Science Foundation of China (Nos.81471110 and 81671184), and the Assistance Program of Xijing Hospital (No.XJZT18MJ19). We thank the China Brain Bank, Zhejiang University, for providing the human brain tissues, and we thank the included stroke patients and their families for their trust.

AUTHOR CONTRIBUTIONS

L.X. and Y.L. conceived, designed, and supervised the study. Y.C., H.G., Z.F., and X.Z. performed most of the experiments. Y.C. established the OGD/R model and completed most of the cell-based experiments. H.G. performed the TTC staining, Nissl staining, and behavioral tests. Z.F. performed the immunoblotting, RT-qPCR, and immunofluorescence staining. X.Z. performed intracerebroventricular injection. W.T. performed the cell-metabolism-associated assays using the Seahorse system. D.W. and X.J. performed the experiments involving rhesus monkeys. T.G. isolated primary astrocytes and neurons. S.W. performed the MCAO surgery on rodents. A.Y. and L.T. analyzed the data. L.X., Y.L., and H.D. drafted and revised the manuscript.

DECLARATION OF INTERESTS

The authors declare no competing interests.

Received: October 17, 2019
Revised: February 27, 2020
Accepted: April 30, 2020
Published: May 22, 2020

REFERENCES

Ashrafi, G., Wu, Z., Farrell, R.J., and Ryan, T.A. (2017). GLUT4 mobilization supports energetic demands of active synapses. Neuron *93*, 606–615.e3.

Augé, E., Pelegrí, C., Manich, G., Cabezón, I., Guinovart, J.J., Duran, J., and Vilaplana, J. (2018). Astrocytes and neurons produce distinct types of polyglucosan bodies in Lafora disease. Glia *66*, 2094–2107.

Bak, L.K., Walls, A.B., Schousboe, A., and Waagepetersen, H.S. (2018). Astrocytic glycogen metabolism in the healthy and diseased brain. J. Biol. Chem. *293*, 7108–7116.

Bar, B., and Biller, J. (2018). Select hyperacute complications of ischemic stroke: cerebral edema, hemorrhagic transformation, and orolingual angioedema secondary to intravenous alteplase. Expert Rev. Neurother. *18*, 749–759.

Barbosa, E.H., Vallim, J.H., Lachat, J.J., and de Castro, V.L. (2016). Assessments of motor abnormalities on the grid-walking and foot-fault tests from undernutrition in wistar rats. J. Mot. Behav. *48*, 5–12.

Barnett, D., Hall, J., and Haab, B. (2019). Automated identification and quantification of signals in multichannel immunofluorescence images: the SignalFinder-IF platform. Am. J. Pathol. *189*, 1402–1412.

Bertrand, L., Horman, S., Beauloye, C., and Vanoverschelde, J.L. (2008). Insulin signalling in the heart. Cardiovasc. Res. *79*, 238–248.

Brenner, M., Kisseberth, W.C., Su, Y., Besnard, F., and Messing, A. (1994). GFAP promoter directs astrocyte-specific expression in transgenic mice. J. Neurosci. *14*, 1030–1037.

Brewer, M.K., and Gentry, M.S. (2019). Brain glycogen structure and its associated proteins:

past, present and future. Adv. Neurobiol. *23*, 17–81.

Bushong, E.A., Martone, M.E., Jones, Y.Z., and Ellisman, M.H. (2002). Protoplasmic astrocytes in CA1 stratum radiatum occupy separate anatomical domains. J. Neurosci. *22*, 183–192.

Cai, W., Xue, C., Sakaguchi, M., Konishi, M., Shirazian, A., Ferris, H.A., Li, M.E., Yu, R., Kleinridders, A., Pothos, E.N., et al. (2018). Insulin regulates astrocyte gliotransmission and modulates behavior. J. Clin. Invest. *128*, 2914–2926.

Dienel, G.A. (2019). Brain glucose metabolism: integration of energetics with function. Physiol. Rev. *99*, 949–1045.

Dienel, G.A., and Cruz, N.F. (2015). Contributions of glycogen to astrocytic energetics during brain activation. Metab. Brain Dis. *30*, 281–298.

Dienel, G.A., and Rothman, D.L. (2019). Glycogenolysis in cerebral cortex during sensory stimulation, acute hypoglycemia, and exercise: impact on astrocytic energetics, aerobic glycolysis, and astrocyte-neuron interactions. Adv. Neurobiol. *23*, 209–267.

Dukhande, V.V., Rogers, D.M., Romá-Mateo, C., Donderis, J., Marina, A., Taylor, A.O., Sanz, P., and Gentry, M.S. (2011). Laforin, a dual specificity phosphatase involved in Lafora disease, is present mainly as monomeric form with full phosphatase activity. PLoS One *6*, e24040.

Duran, J., Gruart, A., Varea, O., López-Soldado, I., Delgado-García, J.M., and Guinovart, J.J. (2019). Lack of neuronal glycogen impairs memory formation and learning-dependent synaptic plasticity in mice. Front. Cell. Neurosci. *13*, 374.

Fernandez, A.M., Hernandez-Garzón, E., Perez-Domper, P., Perez-Alvarez, A., Mederos, S., Matsui, T., Santi, A., Trueba-Saiz, A., García-Guerra, L., Pose-Utrilla, J., et al. (2017). Insulin regulates astrocytic glucose handling through cooperation with IGF-I. Diabetes *66*, 64–74.

Folbergrova, J., Katsura, K.I., and Siesjo, B.K. (1996). Glycogen accumulated in the brain following insults is not degraded during a subsequent period of ischemia. J. Neurol. Sci. *137*, 7–13.

GBD 2015 DALYs and HALE Collaborators (2016). Global, regional, and National disability-adjusted life-years (DALYs) for 315 diseases and injuries and healthy life expectancy (HALE), 1990-2015: a systematic analysis for the global burden of disease study 2015. Lancet *388*, 1603–1658.

GBD 2015 Mortality and Causes of Death Collaborators (2016). Global, regional, and national life expectancy, all-cause mortality, and cause-specific mortality for 249 causes of death, 1980-2015: a systematic analysis for the global burden of disease study 2015. Lancet *388*, 1459–1544.

Gentry, M.S., Worby, C.A., and Dixon, J.E. (2005). Insights into Lafora disease: malin is an E3 ubiquitin ligase that ubiquitinates and promotes the degradation of laforin. Proc. Natl. Acad. Sci. U S A *102*, 8501–8506.

Guan, T., Qian, Y., Tang, X., Huang, M., Huang, L., Li, Y., and Sun, H. (2011). Maslinic acid, a natural inhibitor of glycogen phosphorylase, reduces cerebral ischemic injury in hyperglycemic rats by GLT-1 up-regulation. J. Neurosci. Res. *89*, 1829–1839.

Gurer, G., Gursoy-Ozdemir, Y., Erdemli, E., Can, A., and Dalkara, T. (2009). Astrocytes are more resistant to focal cerebral ischemia than neurons and die by a delayed necrosis. Brain Pathol. *19*, 630–641.

Hankey, G.J. (2017). Stroke. Lancet *389*, 641–654.

Hossain, M.I., Roulston, C.L., and Stapleton, D.I. (2014). Molecular basis of impaired glycogen metabolism during ischemic stroke and hypoxia. PLoS One *9*, e97570.

Kajihara, H., Tsutsumi, E., Kinoshita, A., Nakano, J., Takagi, K., and Takeo, S. (2001). Activated astrocytes with glycogen accumulation in ischemic penumbra during the early stage of brain infarction: immunohistochemical and electron microscopic studies. Brain Res. *909*, 92–101.

Kirsch, W.M., and Leitner, J.W. (1967). Glycolytic metabolites and co-factors in human cerebral cortex and white matter during complete ischemia. Brain Res. *4*, 358–368.

Krewson, E.A., Sanderlin, E.J., Marie, M.A., Akhtar, S.N., Velcicky, J., Loetscher, P., and Yang, L.V. (2020). The proton-sensing GPR4 receptor regulates paracellular gap formation and permeability of vascular endothelial cells. iScience *23*, 100848.

Long, D.M., Mossakowski, M.J., and Klatzo, I. (1972). Glycogen accumulation in spinal cord motor neurons due to partial ischemia. Acta Neuropathol. *20*, 335–347.

Lowry, O.H., and Passonneau, J.V. (1964). The relationships between substrates and enzymes of glycolysis in brain. J. Biol. Chem. *239*, 31–42.

Lowry, O.H., Passonneau, J.V., Hasselberger, F.X., and Schulz, D.W. (1964). Effect of ischemia on known substrates and cofactors of the glycolytic pathway in brain. J. Biol. Chem. *239*, 18–30.

Müller, M.S., Fox, R., Schousboe, A., Waagepetersen, H.S., and Bak, L.K. (2014). Astrocyte glycogenolysis is triggered by store-operated calcium entry and provides metabolic energy for cellular calcium homeostasis. Glia *62*, 526–534.

Ma, H., Campbell, B.C.V., Parsons, M.W., Churilov, L., Levi, C.R., Hsu, C., Kleinig, T.J., Wijeratne, T., Curtze, S., Dewey, H.M., et al. (2019). Thrombolysis guided by perfusion imaging up to 9 hours after onset of stroke. N. Engl. J. Med. *380*, 1795–1803.

Magistretti, P.J., and Allaman, I. (2015). A cellular perspective on brain energy metabolism and functional imaging. Neuron *86*, 883–901.

Masuda, S., Chikuma, M., and Sasaki, R. (1997). Insulin-like growth factors and insulin stimulate erythropoietin production in primary cultured astrocytes. Brain Res. *746*, 63–70.

Mishra, N., Lata, S., Deshmukh, P., Kamat, K., Surolia, A., and Banerjee, T. (2018). Insulin signaling pathway protects neuronal cell lines by Sirt3 mediated IRS2 activation. Biofactors *44*, 224–236.

Moore, M.C., Coate, K.C., Winnick, J.J., An, Z., and Cherrington, A.D. (2012). Regulation of hepatic glucose uptake and storage *in vivo*. Adv. Nutr. *3*, 286–294.

Mrsulja, B.B., Mrsulja, B.J., Ito, U., Walker, J.T., Jr., Spatz, M., and Klatzo, I. (1975). Experimental cerebral ischemia in Mongolian gerbils. II. Changes in carbohydrates. Acta Neuropathol. *33*, 91–103.

Mrsulja, B.J., Spatz, M., Walker, J.T., Jr., and Klatzo, I. (1979). Histochemical investigation of the Mongolian gerbil's brain during unilateral ischemia. Acta Neuropathol. *46*, 123–131.

Mullins, M.E. (2006). Modern emergent stroke imaging: pearls, protocols, and pitfalls. Radiol. Clin. North Am. *44*, 41–62, vii–viii.

Odell, I.D., and Cook, D. (2013). Immunofluorescence techniques. J. Invest. Dermatol. *133*, e4.

Oe, Y., Baba, O., Ashida, H., Nakamura, K.C., and Hirase, H. (2016). Glycogen distribution in the microwave-fixed mouse brain reveals heterogeneous astrocytic patterns. Glia *64*, 1532–1545.

Pearson-Leary, J., Jahagirdar, V., Sage, J., and McNay, E.C. (2018). Insulin modulates hippocampally-mediated spatial working memory via glucose transporter-4. Behav. Brain Res. *338*, 32–39.

Pederson, B.A. (2019). Structure and regulation of glycogen synthase in the brain. Adv. Neurobiol. *23*, 83–123.

Pundik, S., Xu, K., and Sundararajan, S. (2012). Reperfusion brain injury: focus on cellular bioenergetics. Neurology *79*, S44–S51.

Ramagiri, S., and Taliyan, R. (2017). Remote limb ischemic post conditioning during early reperfusion alleviates cerebral ischemic reperfusion injury via GSK-3beta/CREB/BDNF pathway. Eur. J. Pharmacol. *803*, 84–93.

Saez, I., Duran, J., Sinadinos, C., Beltran, A., Yanes, O., Tevy, M.F., Martínez-Pons, C., Milán, M., and Guinovart, J.J. (2014). Neurons have an active glycogen metabolism that contributes to tolerance to hypoxia. J. Cereb. Blood Flow.Metab. *34*, 945–955.

Taylor, S.S., Ilouz, R., Zhang, P., and Kornev, A.P. (2012). Assembly of allosteric macromolecular switches: lessons from PKA. Nat. Rev. Mol. Cell Biol. *13*, 646–658.

Tracey, W.R., Treadway, J.L., Magee, W.P., Sutt, J.C., McPherson, R.K., Levy, C.B., Wilder, D.E., Yu, L.J., Chen, Y., Shanker, R.M., et al. (2004). Cardioprotective effects of ingliforib, a novel glycogen phosphorylase inhibitor. Am. J. Physiol. Heart Circ. Physiol. *286*, H1177–H1184.

Wang, H., Kumar, A., Lamont, R.J., and Scott, D.A. (2014). GSK3beta and the control of infectious bacterial diseases. Trends Microbiol. *22*, 208–217.

Xu, J., Song, D., Bai, Q., Zhou, L., Cai, L., Hertz, L., and Peng, L. (2014). Role of glycogenolysis in

stimulation of ATP release from cultured mouse astrocytes by transmitters and high K+ concentrations. ASN Neuro *6*, e00132.

Xu, J., Song, D., Xue, Z., Gu, L., Hertz, L., and Peng, L. (2013). Requirement of glycogenolysis for uptake of increased extracellular K+ in astrocytes: potential implications for K+ homeostasis and glycogen usage in brain. Neurochem. Res. *38*, 472–485.

Xu, L., and Sun, H. (2010). Pharmacological manipulation of brain glycogenolysis as a therapeutic approach to cerebral ischemia. Mini Rev. Med. Chem *10*, 1188–1193.

Yin, A., Guo, H., Tao, L., Cai, G., Wang, Y., Yao, L., Xiong, L., Zhang, J., and Li, Y. (2019). NDRG2 protects the brain from excitotoxicity by facilitating interstitial glutamate uptake. Transl. Stroke Res. https://doi.org/10.1007/s12975–12019–00708–12979.

Zhang, H.X., Zang, Y.M., Huo, J.H., Liang, S.J., Zhang, H.F., Wang, Y.M., Fan, Q., Guo, W.Y., Wang, H.C., and Gao, F. (2006). Physiologically tolerable insulin reduces myocardial injury and improves cardiac functional recovery in myocardial ischemic/reperfused dogs. J. Cardiovasc. Pharmacol. *48*, 306–313.

Zhang, L., Schallert, T., Zhang, Z.G., Jiang, Q., Arniego, P., Li, Q., Lu, M., and Chopp, M. (2002). A test for detecting long-term sensorimotor dysfunction in the mouse after focal cerebral ischemia. J. Neurosci. Methods *117*, 207–214.

Zhang, Z., Yan, J., and Shi, H. (2013). Hyperglycemia as a risk factor of ischemic stroke. J. Drug Metab.Toxicol. *4*, 153.

Zois, C.E., and Harris, A.L. (2016). Glycogen metabolism has a key role in the cancer microenvironment and provides new targets for cancer therapy. J. Mol. Med. (Berl.) *94*, 137–154.

iScience, Volume *23*

Supplemental Information

Glycogenolysis Is Crucial for Astrocytic Glycogen Accumulation and Brain Damage after Reperfusion in Ischemic Stroke

Yanhui Cai, Haiyun Guo, Ze Fan, Xinlei Zhang, Di Wu, Wenhong Tang, Tingting Gu, Shiquan Wang, Anqi Yin, Liang Tao, Xunming Ji, Hailong Dong, Yan Li, and Lize Xiong

TRANSPARENT METHODS

Human tissues

Brain tissues from stroke patients were obtained from the China Brain Bank, Zhejiang University (Hangzhou, China). The patient information is presented in Table S1. The human tissues were obtained and used in accordance with the ethical standards of the Zhejiang University Ethics Committee (ID: 2019-001). Informed consent was received from participants prior to inclusion in the study. The brain tissues of stroke patients were cut to identify the different regions including the core infarction area and penumbra area and then were frozen with liquid nitrogen. The postmortem interval (PMI) was about 30-40 min and the time for dissection to obtain the penumbra tissue was about 20 min.

Monkey tissues

Brain tissues from eight- to ten-year-old male rhesus monkeys (*Macaca mulatta*, weighing 7.8-10.5 kg) subjected to I/R stress were obtained from Xuanwu Hospital, Capital Medical University (Beijing, China). Animal studies were conducted in accordance with national guidelines and in compliance with the United States Public Health Service's Policy on the Humane Care and Use of Laboratory Animals. The rhesus monkey experiments were approved by the Animal Use and Care Board of the Institute of Laboratory Animal Sciences, Capital Medical University. A monkey stroke model was constructed according to a previous study (Wu et al., 2018). Briefly, anesthesia was induced with intramuscular ketamine (10 mg/kg) and

maintained intravenously with propofol (300 μg/kg/min). One day before the operation, blood was drawn from the femoral vein and allowed to clot. During the operation, a microcatheter with a guiding wire was introduced into the guiding catheter and navigated into the distal right middle cerebral artery. Then, the clot was transferred into the microcatheter and flushed into the distal right middle cerebral artery with 2 mL of saline. The occlusion of the cerebral blood flow was confirmed with an angiogram. The ischemia was maintained for 3 h before thrombolysis using urokinase and the reperfusion was confirmed by an angiogram. During the operation, the vital signs of the monkeys were continuously monitored with interventional devices. The time between thrombolysis and sacrifice was 12 h and the brain tissues were cut to identify the different regions including the core infarction area and penumbra area and then was frozen with liquid nitrogen, which needed about 20 min.

Mice

Four-week-old male C57BL/6J mice, one-day-old neonatal C57BL/6J pups and embryonic day 15-16 female C57BL/6J mice were purchased from the Experimental Animal Center of the Fourth Military Medical University. Astrocyte-specific brain isoform of glycogen phosphorylase (PYGB) knock-in mice were customized by Cyagen (Santa Clara, USA). The rodent experiments were approved by the Animal Care Committee of the Fourth Military Medical University. The mice were housed in groups of four with *ad libitum* access to water and food in standard breeding cages at 23 ± 1 °C. All experiments and data analyses were conducted by investigators who were blinded to the animal groups, which were determined by randomization.

Reagents

Insulin (I9278, Sigma-Aldrich), 8-Br-cAMP (ab141448, Abcam) and 1,4-dideoxy-1,4-imino-D-arabinitol (DAB, D1542, Sigma-Aldrich) were used in this study.

Primary neuron and astrocyte culture

To obtain primary astrocytes, one-day-old neonatal C57BL/6J pups were sterilized with 75% ethanol and decapitated. The cortices were removed from the skulls on ice. The meninges were peeled from the brains under a microscope on ice, and the tissues were digested with trypsin (25200056, Thermo Fisher Scientific) at 37 °C for 10 min. The trypsin activity was terminated with Dulbecco's modified Eagle's medium (DMEM, SH30022, HyClone, 25 mM glucose) with 15% fetal bovine serum (FBS, 16140071, Thermo Fisher Scientific), and the mixture was filtered through a sterile 200-mesh screen. The filtrate was centrifuged at 800 rpm for 10 min, and the cells were seeded onto poly-D-lysine (0.1 mg/mL, P0296, Sigma-Aldrich)-coated flasks at a density of 10000 cells per cm^2. The cells were maintained for 7 days with culture medium changes every 3 days and were then shaken for 19 h at 190 rpm at 37 °C to remove oligodendrocytes and microglial cells. The astrocytes were cultured for 21 days with no extra stimulating factors for maturation, and the maturity of cultured astrocytes was determined by $S100\beta^+/GFAP^+$ via immunofluorescence (Raponi et al., 2007), but no enzymatic or other functional measures of maturation were evaluated. As shown in Figure S14A, the percentage of

mature astrocytes was 85.5% on day 21. Astrocytes were harvested according to the detection time after oxygen-glucose deprivation/reoxygenation (OGD/R).

Primary neurons were obtained from the cortices of embryonic day 15-16 C57BL/6J embryos. The procedure was the same as that used to prepare primary astrocytes except that the digestion time for brain tissues after removal of the meninges was 20 min at 37 °C. The culture medium used for neurons was neurobasal medium (21103049, Thermo Fisher Scientific, 25 mM glucose) with added B-27 (2%, 17504044, Thermo Fisher Scientific) and glutamine (1%, 35050061, Thermo Fisher Scientific). Neuron medium was changed every 4 days by replacing half of the old medium with fresh medium to ensure consistent conditioning of the culture. The neurons were cultured for 14 days with no extra stimulating factors for maturation, and the maturity of cultured neurons was identified by $MAP2^{+}/DCX^{-}$ via immunofluorescence (Cho et al., 2018), but no enzymatic or other functional measures of maturation were evaluated. As shown in Figure S14B, the percentage of mature neurons was 78.7% on day 14.

The astrocyte-neuron coculture system was established using hanging inserts with porous membranes (3 μm, MCSP24H48, Millipore). The distance from the astrocytic membrane to the neuronal layer was 0.15 cm, and the volume of coculture medium was 400 μL. The coculture medium consisted of neurobasal medium (25 mM glucose) with 15% FBS, 2% B-27 and 1% glutamine. 14-day astrocytes and 7-day neurons were cocultured for 7 days before OGD/R stress. Cocultured neurons were harvested according to the detection time after OGD/R.

I/R model in mice

A middle cerebral artery occlusion/reperfusion (MCAO/R) model was established to mimic I/R in mice. Male C57BL/6J mice (8 weeks old) were anesthetized with 1.4% isoflurane. A tiny incision was made in the skin of each mouse at the midline of the anterior neck, and the muscles were removed under a surgical microscope. Then, a monofilament (MSMC23B104PK100, RWD Life Science) was introduced into the internal carotid artery through a small incision and extended into the right middle cerebral artery. After 60 min, the filament was withdrawn, and the wound was sutured. During the operation, the temperature was controlled by keeping the mice on a heating plate at 37 °C until they regained full consciousness. The mice in the sham group underwent the same surgical procedures as the MCAO group except for artery occlusion.

The frontal cortex area 1 on the side of ipsilateral hemisphere, which is from bregma to (bregma – 1 mm) in the coronal plane, was considered as the ischemic penumbra during transient MCAO in mice (Chen et al., 2019; Li and Zuo, 2011). The mice were anesthetized with intraperitoneal administration of pentobarbital sodium (150 mg/kg, P-010, Sigma-Aldrich) before decapitation.

I/R model in vitro

In this study, the classic OGD/R model was established to mimic I/R after stroke using a humidified 37 °C hermetic chamber (Billups-Rothenberg). After washing with phosphate-buffered saline (PBS), the culture medium was replaced with glucose-free DMEM (A1443001, Thermo Fisher Scientific) for astrocytes and glucose-free neurobasal medium (A2477501, Thermo Fisher Scientific) for coculture. Then, the cells were moved into a chamber containing

an anaerobic gas mixture (5% CO_2 and 95% N_2). The duration of OGD was 2 h for most *in vitro* experiments. On the basis of 2 h of OGD, additional treatment with 1 h of OGD without reoxygenation was used only to continuously detect the alterations of key enzymes in glycogen metabolism during OGD/R stress, as shown for one group in Figures S2 and S8. After the cells were removed from the chamber, the glucose-free medium was replaced with complete culture medium (DMEM with 15% FBS for astrocytes and neurobasal medium with 15% FBS, 2% B-27 and 1% glutamine for cocultures). The non-OGD groups also received culture medium changes (containing 25 mM glucose) before and after OGD stress. The medium change after OGD was regarded as the last feeding for cultured astrocytes and cocultured neurons, and the interval time between the last feeding and biochemical assays was dependent on the detection time.

Seahorse analysis

Astrocytes (60000 cells per well) were plated into an XF24 Cell Culture Microplate (100777-004, Seahorse Bioscience). A Seahorse XF24 Analyzer was used to analyze the extracellular acidification rate (ECAR) and oxygen consumption rate (OCR) according to the protocols for the Glycolysis Stress Test Kit (103020-100, Seahorse Bioscience) and Cell Mito Stress Test Kit (103015-100, Seahorse Bioscience). The final concentrations of the activators/inhibitors were as follows: glucose, 10 mM; oligomycin, 0.5 μM; antimycin A, 2 μM; carbonyl cyanide-4-phenylhydrazone (FCCP), 0.5 μM; and 2-deoxy-d-glucose (2-DG), 50 mM. The glycolytic capacity and ATP production were determined by subtracting the corresponding OCR or ECAR measurement values.

Corner test

Mice were placed in a 30° corner. One successful turning trial was counted when a mouse stood on its hind limbs and turned around to the right or left in the corner to exit. Whether the mouse turned right or left was recorded for 10 trials for each animal, with at least 30 s between trials. The score was calculated as the number of right body turns in 10 trials (Zhang et al., 2002).

Grid-walking test

An elevated metal grid (40 × 20 cm^2, each grid cell 2 × 2 cm^2, height 50 cm) was used to assess the activity and walking performance of the mice. The grid apparatus was located in a sound-attenuated room. Performance was recorded for 60 s using a video camera located beside the apparatus at an angle of approximately 20 to 40 degrees. A foot slip was recorded when one paw completely missed a bar, with the limb falling between the bars, or when the paw was correctly placed on the bar but slipped off during weight bearing (shown in Movie S1). The total steps of the left forelimb and hind limb were counted, and the percentage of foot fault was measured by dividing the number of foot slips of the left forelimb and left hind limb by the total number of left steps taken within 60 s.

Immunofluorescence staining

The mice were deeply anesthetized with intraperitoneal administration of pentobarbital sodium (150 mg/kg) and transcardially perfused with saline followed by 4% paraformaldehyde (158127,

Sigma-Aldrich) in PBS. The cerebrum was removed and postfixed overnight with 4% paraformaldehyde and then cryoprotected with 20% and 30% sucrose (S9378, Sigma-Aldrich) in PBS for 1 day each. The brains were frozen, and ten coronal brain sections (12 μm) at approximately bregma - 0.5 mm were collected on slides with a cryostat and blocked with serum. The incubation time was 12 h at 4 °C for primary antibodies and 2 h for secondary antibodies. DAPI (300 nM, C001, GeneCopoeia) was applied to visualize all cells, and a confocal microscope (Olympus) was used to capture images. The fluorescence intensity of the colocalization area and S100β$^+$ area was calculated using ImageJ software. The antibodies used for immunofluorescence staining are shown in Table S2. The spectral range for Alexa Fluor 488 (Thermo Fisher Scientific) is 488-493 nm and for Alexa Fluor 594 (Thermo Fisher Scientific) is 550-594 nm. The excitation wavelengths for target proteins in green is 488 nm and for target proteins in red is 594 nm. The relative fluorescence intensity was calculated as the percentage of fluorescence intensity in the colocalization area divided by the fluorescence intensity in the S100β$^+$ area.

Immunoblotting

The brain tissue lysates and astrocyte lysates were prepared in RIPA lysis and extraction buffer (89901, Thermo Fisher Scientific) containing a protease and phosphatase inhibitor cocktail (1%, 78442, Thermo Fisher Scientific). The protein concentrations were measured with a BCA Protein Assay Kit (23227, Thermo Fisher Scientific), and the samples were separated by SDS-PAGE and transferred onto 0.2 μm PVDF membranes (88520, Thermo Fisher Scientific). The band densities

were captured and analyzed with the software program Image Lab 4.1 (Bio-Rad). The antibodies used for immunoblotting are shown in Table S2.

Preparation and characterization of a polyclonal antibody targeting phosphorylated PYGB (Ser14)

An antibody targeting phosphorylated PYGB (Ser14) is still commercially unavailable and was synthesized by Genecreate Biological Engineering (Wuhan, China). In brief, a 14-amino acid phosphorylated peptide (TDSERQKQI-pS-VRGI) predicted by epitope analysis software was chemically synthesized and used as an immunogen for subcutaneous injection into male rabbits at 2-week intervals. After 4 immunizations, the antiserum was harvested and subjected to phosphorylated affinity purification twice, followed by six times of nonphosphorylated affinity purification. The dilution ratio of the synthesized phosphorylated antibody for specifically recognizing phosphorylated PYGB was verified by Genecreate Biological Engineering using an indirect enzyme-linked immunosorbent assay (ELISA) towards phosphorylated and nonphosphorylated peptides (Figure S4A). As shown in Figure S4A, when the dilution ratio of phosphorylated PYGB antibody was 1:500, the absorbance of phosphorylated PYGB antibody integration with unphosphorylated peptides was close to 0, suggesting the phosphorylated PYGB antibody could specifically recognize the phosphorylated PYGB at the dilution ratio of 1:500 (Bergmann et al., 2017). Additionally, when the dilution ratio was 1:500, the phosphorylated PYGB antibody could recognized the phosphorylated PYGB in immunofluorescence assays as well (Figure S4B).

Quantitative reverse transcription polymerase chain reaction (RT-qPCR)

Total RNA in astrocytes was obtained using an RNA Extraction Kit (9767, Takara Bio Inc.), and a NanoDrop 2000 spectrophotometer (Thermo Fisher Scientific) was used to determine the RNA concentrations. Then, the RNA was converted into cDNA with PrimeScript^{TM} RT Master Mix (RR036A, Takara Bio Inc.). RT-qPCR was conducted on an iQ5 Real-Time PCR Detection System (Bio-Rad) with SYBR (RR820A, Takara Bio Inc.). The primers and corresponding accession numbers used for RT-qPCR are shown in Table S3.

PYGB overexpression and CRISPR/Cas9-mediated knockdown in vitro

Preliminary experiments used DAB, a potent inhibitor of GP and GS activity in liver (Walls et al., 2008), to reduce the activity of GP in cultured neurons and astrocytes. However, neuronal viability was selectively affected compared with that of astrocytes at DAB concentrations exceeding 10 μM (Figure S15), and even 300 μM DAB was reported to not inhibit GP in cultured astrocytes (Walls et al., 2008). Consequently, an alternative approach was used in this study.

A lentivirus driving the expression of PYGB and a lentivirus with an sgRNA (ATGCGACGAAGCCACTTATC) against the *pygb* gene (GenBank: NM_153781) were constructed individually by GeneChem Ltd. (Shanghai, China). A mock vector without the *pygb* gene and a scrambled sgRNA (CGCTTCCGCGGCCCGTTCAA) were constructed as negative controls.

Before infection, astrocytes were cultured to 70% confluency. The lentiviruses were mixed with culture medium at a multiplicity of infection of 100 for 72 h. The success of lentivirus-mediated upregulation or silencing of *pygb* was confirmed by immunoblotting, biochemical assays and with a Knockdown and Mutation Detection Kit (MB001-1004, GeneChem Ltd.).

Intracerebroventricular injection

A cannula was placed into the lateral ventricle one week before MCAO, and insulin was injected into the lateral ventricle. Briefly, each mouse was administered 1.4% isoflurane anesthesia through a facemask and placed in a stereotaxic head frame (Stoelting). A 1.0 mm burr hole was made with a dental trephine drill (NSK Ltd.) after retracting the scalp. The coordinates of the stereotaxic apparatus were as follows: 1.4 mm deep, 1.0 mm to left of the midline and 0.22 mm posterior to the bregma. Then, 2 μL of insulin was infused into the brain over 20 min using a Hamilton syringe. The needle was left in place for an additional 30 min to prevent reflux before removal, and the craniotomy was sealed with quick self-curing acrylic resin (Yamahachi Dental Mfg.). Then, the scalp was sutured closed. An electronic thermostat-controlled warming blanket was used to keep the body temperature of the mouse at 37 ± 0.5 °C throughout the experimental and recovery periods.

Considering that the total volume of cerebrospinal fluid is approximately 10-20 μL in an 8-week-old mouse (Atangana et al., 2015; Šakić, 2019) and the volume of insulin injection into the lateral ventricle is 2 μL, insulin (10 μM) was injected into the lateral ventricle immediately

after reperfusion to achieve a final concentration of approximately 1 μM in the cerebrospinal fluid.

Astrocytic PYGB knockdown rodent model

AAVs with an astrocyte-specific GFAP promoter (Brenner et al., 1994) used to drive the short hairpin RNA (shRNA) containing 19 nucleotides (GAGGTCCCTTGAAGCCATA) specific for the *pygb* gene followed by a FLAG tag were purchased from GeneChem Ltd. 2 μL of AAV (5×10^{12} v.g./mL) was injected into the lateral ventricle three weeks before MCAO, as described above for the intracerebroventricular injection. The coordinates of the stereotaxic apparatus were as follows: 1.0 mm to the right of the midline, 0.22 mm posterior to the bregma and 1.4 mm deep.

Triphenyl tetrazolium chloride (TTC) staining

The mice were deeply anesthetized via intraperitoneal administration of pentobarbital sodium (150 mg/kg) and transcardially perfused with saline. The cerebrum was removed from the skulls, and the brain tissues were continuously cut into coronal slices at 1 mm intervals and immersed in 2% TTC solution (103126, MP Biomedicals) for 20 min at 37 °C. The TTC-stained areas (red) indicate the nonischemic regions, and the white areas show the ischemic regions. The lesion area was evaluated using ImageJ software. The infarct volume was calculated in arbitrary units (pixels) as the following ratio: (area of the contralateral hemisphere – nonlesion area in the ipsilateral hemisphere) / area of the contralateral hemisphere.

Nissl staining

The mice were deeply anesthetized via intraperitoneal administration of pentobarbital sodium (150 mg/kg) and transcardially perfused with saline followed by 4% paraformaldehyde in PBS. The cerebrum was removed, postfixed overnight with 4% paraformaldehyde and then cryoprotected with 20% and 30% sucrose in PBS for 1 day each. Coronal brain sections (20 μm) were cut with a cryostat, and one out of every 20 sections was collected on a slide for assessment of cerebral injury. The slides were stained with cresyl violet (1%, C5042, Sigma-Aldrich) for 10 min. The lesion area was evaluated using ImageJ software. The infarct volume was calculated in arbitrary units (pixels) as the following ratio: (area of the contralateral hemisphere – nonlesion area in the ipsilateral hemisphere) / area of the contralateral hemisphere.

Electron microscopy analysis

The mice were deeply anesthetized via intraperitoneal administration of pentobarbital sodium (150 mg/kg) and transcardially perfused with saline followed by 2% glutaraldehyde in 0.1 M sodium cacodylate buffer (16536-15, Electron Microscopy Sciences). Then, the cerebrum was removed from the skull. The cultured neural cells were scraped with a cell scraper, collected in a prechilled microcentrifuge tube and centrifuged at 1,000 rpm for 15 min at 4 °C. Then, the neural cell pellets or brain tissues from mice were fixed with 2% glutaraldehyde in 0.1 M sodium cacodylate buffer for 1 h and postfixed with 1% OsO_4 (419494, Sigma-Aldrich) in 4% paraformaldehyde buffer for 1 h at 4 °C. After dehydration with graded ethanol, the samples

were embedded, heated at 60 °C for 48 h and cut into 50 nm ultrathin sections with an ultramicrotome (LKB Inc.). The ultrathin slices were stained with saturated lead citrate and uranyl acetate and then observed using a transmission electron microscope (JEOL Ltd.).

Biochemical glycogen quantitative assay

Human brain tissues in the penumbra were preserved in liquid nitrogen. Monkeys were deeply anesthetized via intravenous administration of pentobarbital sodium (100 mg/kg) and euthanized. The cerebrum was removed from the skulls, and brain tissues in the penumbra were frozen with liquid nitrogen. The mice were decapitated, and brain tissues in the penumbra were frozen with liquid nitrogen. 10 mg brain tissues were homogenized with 200 μL 30% KOH on ice and the homogenates were then boiled for 10 min to inactivate enzymes. The boiled samples were centrifuged at 12000 rpm for 10 min at 4 °C to remove insoluble materials and the supernatant was ready for the assay using a Glycogen Assay Kit (K648, BioVision), and the results were normalized to the protein levels in homologous samples.

For cultured astrocytes, the culture medium was discarded, and cells were washed with PBS buffer, lysed with 30% KOH and scraped into eppendorf tubes. Samples were boiled and centrifuged with 12000 rpm for 10 min at 4 °C to remove insoluble materials and the supernatant was ready for the assay using a Glycogen Assay Kit.

The lag time between death and removal of penumbra tissue to liquid nitrogen was approximately 60 min for each patient (The PMI was approximately 30-40 min, and the time for dissection to obtain the penumbra tissue was approximately 20 min). The lag time between death

and removal of penumbra tissue to liquid nitrogen was approximately 20 min for each monkey. The lag time between death and removal of penumbra tissue to liquid nitrogen was approximately 30 s for each mouse. The lag time between medium removal and glycogen dissolution into lysis buffer was approximately 30 s for astrocytes.

Periodic acid-Schiff (PAS) staining

Paraffin sections of human brain tissues in the penumbra were obtained from the China Brain Bank. Monkeys were deeply anesthetized with intravenous administration of pentobarbital sodium (100 mg/kg) and euthanized. The cerebrum was removed from the skulls, and the brain tissues in the penumbra were postfixed with 4% paraformaldehyde. The mice were deeply anesthetized with intraperitoneal administration of pentobarbital sodium (150 mg/kg) and transcardially perfused with PBS followed by 4% paraformaldehyde in PBS. The cerebrum was removed and postfixed overnight with 4% paraformaldehyde. For cultured astrocytes, cells were seeded onto poly-D-lysine-coated slices and fixed with 4% paraformaldehyde in PBS for 1 h at room temperature. After washing with PBS, the slices were blocked with 3% H_2O_2 in methanol for 10 min at room temperature, followed by incubation in 0.1% Triton X-100 in 0.1% sodium citrate for permeabilization for 2 min on ice.

PAS staining for brain tissues of humans, monkeys and mice and cultured astrocytes was performed according to the instructions of a PAS Stain Kit (ab150680, Abcam).

Blood glucose analysis

The venous blood glucose levels in mice were determined using a blood glucose meter (OneTouch Ultra).

Preparation of lysates from cultured astrocytes for enzyme activity assays

Adherent astrocytes grew to 90% confluency and were dissociated with lysate buffer (GMS12054.2, Genmed Scientifics). The lysis time was 30 min on ice to ensure that enzyme was fully dissolved into lysate buffer. Then, the lysate was collected in a prechilled microcentrifuge tube with a cell scraper and centrifuged at 13,000 rpm for 15 min at 4 °C. The supernatant was used as a source of the enzyme for evaluation, and the protein concentrations were determined using the BCA method.

Glycogen synthase (GS) activity in cultured astrocytes

Active GS activity was determined using a Glycogen Synthase Activity Assay Kit (GMS50500.1, Genmed Scientifics). A substrate solution containing uridine diphosphate glucose (UDPG), phosphoenolpyruvic acid and reduced nicotinamide adenine dinucleotide (NADH) was mixed. Then, an enzyme solution containing the supernatant of cell lysate, pyruvate kinase and lactate dehydrogenase was added to prepare a reaction solution. The UDPG transformed to uridine diphosphate (UDP) represented the activity of GS. Phosphoenolpyruvic acid and UDP as substrates then changed into pyruvate and UTP by pyruvate kinase, and pyruvate was converted to lactate by lactate dehydrogenase in parallel with the transformation of NADH to oxidized nicotinamide adenine dinucleotide (NAD^+), accompanied by decrease in absorbance at 340 nm.

The activity of GS was measured by subtracting the absorbance at 5 min from that at 0 min at 340 nm using a microplate reader (TECAN). The sample preparation was performed on ice, the enzyme reaction procedure was performed at 30 °C, and the results were normalized to the protein levels in homologous samples. The reaction formula is as follows:

$$\text{UDPG} + (\text{Glycogen})_n \xrightarrow{\text{GS}} \text{UDP} + (\text{Glycogen})_{n+1}$$

$$\text{Phosphoenolpyruvate} + \text{UDP} \xrightarrow{\text{Pyruvate kinase}} \text{Pyruvate} + \text{UTP}$$

$$\text{Pyruvate} + \text{NADH} \xrightarrow{\text{Lactate dehydrogenase}} \text{Lactate} + \text{NAD}^+$$

Glycogen phosphorylase (GP) activity in cultured astrocytes

Active GP activity was analyzed with a Glycogen Phosphorylase Activity Assay Kit (GMS50092.1, Genmed Scientifics). The decomposition rate of glycogen to glucose-1-phosphate represented the activity of GP. With phosphoglucomutase and glucose-6-phosphate dehydrogenase, glycogen-derived glucose-1-phosphate was first converted to glucose-6-phosphate, which then transformed into 6-phosphogluconate, and this procedure was combined with conversion of oxidized nicotinamide adenine dinucleotide phosphate ($NADP^+$) to reduced nicotinamide adenine dinucleotide phosphate (NADPH), reflected as the increase in absorbance at 340 nm. The GP activity was measured by subtracting the absorbance at 0 min from that at 5 min at 340 nm using a microplate reader, and the results were normalized to the protein levels in homologous samples. The reaction formula is as follows:

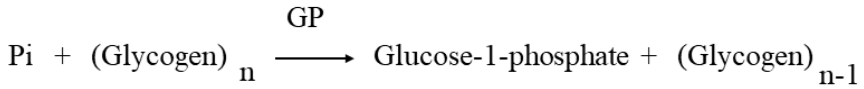

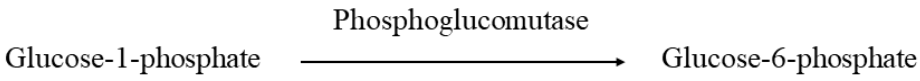

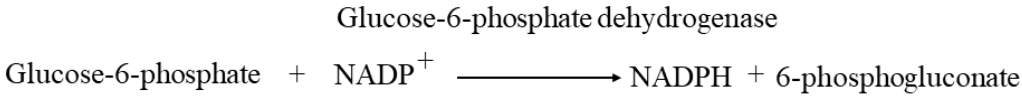

Glycogen phosphorylase kinase (PhK) activity in cultured astrocytes

PhK activity was determined with a Glycogen Phosphorylase Kinase Activity Assay Kit (GMS50618.1, Genmed Scientifics). The substrate solution contained unphosphorylated GP, glycogen, ATP and $NADP^+$. The enzyme solution contained the supernatant of the cell lysate, phosphoglucomutase and glucose-6-phosphate dehydrogenase. The inactive, unphosphorylated GP in the substrate solution was converted to phosphorylated GP (active form) by the cell lysates, and the activity of the phosphorylated, active GP was measured as the rate of degradation of glycogen to glucose-1-phosphate. Next, with phosphoglucomutase and glucose-6-phosphate dehydrogenase, glycogen-derived glucose-1-phosphate was converted to glucose-6-phosphate, which transformed to 6-phosphogluconate, and this procedure was combined with conversion of $NADP^+$ to NADPH, reflected as the increase in absorbance at 340 nm. The PhK activity was measured by subtracting the absorbance at 0 min from that at 10 min at 340 nm

using a microplate reader, and the results were normalized to the protein levels in homologous samples. The reaction formula is as follows:

$$\text{Unphosphorylated GP} + \text{ATP} \xrightarrow{\text{PhK}} \text{Phosphorylated GP} + \text{ADP}$$

$$\text{Pi} + (\text{Glycogen})_{n} \xrightarrow{\text{Phosphorylated GP}} \text{Glucose-1-phosphate} + (\text{Glycogen})_{n-1}$$

$$\text{Glucose-1-phosphate} \xrightarrow{\text{Phosphoglucomutase}} \text{Glucose-6-phosphate}$$

$$\text{Glucose-6-phosphate} + \text{NADP}^{+} \xrightarrow{\text{Glucose-6-phosphate dehydrogenase}} \text{NADPH} + \text{6-phosphogluconate}$$

Protein kinase A (PKA) activity in cultured astrocytes

Briefly, astrocytes were cultured in 6-well plates to reach 90% confluency. After treatment, astrocytes were lysed, and the protein content of each sample was determined with the BCA method. PKA activity of each lysate was evaluated by using the indirect ELISA and following the manufacturer's instructions (ab139435, Abcam). The activity of PKA was measured by the absorbance at 450 nm on a microplate reader.

Glycogen synthase kinase-3α (GSK3α) activity in cultured astrocytes

GSK3α activity was analyzed with a GSK3α Activity Assay Kit (GMS50161.1, Genmed Scientifics). Incubated with the supernatant of the cell lysate and the GSK3β inhibitor thiadiazolidinone-8, the peptide (amino acid sequence: RRAAEELDSRAGSPQL) and ATP first

transformed into phosphorylated peptide and ADP. Then, the substrates phosphoenolpyruvic acid and ADP were converted to pyruvate and ATP by pyruvate kinase, and pyruvate was converted to lactate by lactate dehydrogenase in parallel with the transformation of NADH to NAD^+, accompanied by decrease in absorbance at 340 nm. The activity of GSK3α was measured by subtracting the absorbance at 5 min from that at 0 min at 340 nm using a microplate reader, and the results were normalized to the protein levels in homologous samples. The reaction formula is as follows:

$$\text{ATP} + \text{RRAAEELDSRAGSPQL} \xrightarrow{\text{GSK3}\alpha} \text{ADP} + \text{Phosphorylated-RRAAEELDSRAGSPQL}$$

$$\text{Phosphoenolpyruvate} + \text{ADP} \xrightarrow{\text{Pyruvate kinase}} \text{Pyruvate} + \text{ATP}$$

$$\text{Pyruvate} + \text{NADH} \xrightarrow{\text{Lactate dehydrogenase}} \text{Lactate} + \text{NAD}^+$$

Glycogen synthase kinase-3β (GSK3β) activity in cultured astrocytes

GSK3β activity was measured with a GSK3β Activity Assay Kit (GMS50161.3, Genmed Scientifics). Incubated with the supernatant of the cell lysate and the GSK3α inhibitor Aloisine A, peptide (amino acid sequence: GPHRSTPESRAAV) and ATP transformed into phosphorylated peptide and ADP. Then, the substrates phosphoenolpyruvic acid and ADP were converted to pyruvate and ATP by pyruvate kinase, and pyruvate was converted to lactate by lactate dehydrogenase in parallel with the transformation of NADH to NAD^+, accompanied by

decrease in absorbance at 340 nm. The activity of GSK3β was measured by subtracting the absorbance at 5 min from that at 0 min at 340 nm using a microplate reader, and the results were normalized to the protein levels in homologous samples. The reaction formula is as follows:

$$\text{ATP} + \text{GPHRSTPESRAAV} \xrightarrow{\text{GSK3}\beta} \text{ADP} + \text{Phosphorylated-GPHRSTPESRAAV}$$

$$\text{Phosphoenolpyruvate} + \text{ADP} \xrightarrow{\text{Pyruvate kinase}} \text{Pyruvate} + \text{ATP}$$

$$\text{Pyruvate} + \text{NADH} \xrightarrow{\text{Lactate dehydrogenase}} \text{Lactate} + \text{NAD}^{+}$$

Cell survival analysis

Cell viability was measured with a Cell Counting Kit-8 (CCK-8) assay (96992, Sigma-Aldrich). The incubation time was 1 h for astrocytes and 2 h for neurons. LDH release into the medium was determined with an LDH-Cytotoxicity Colorimetric Assay Kit (K311, BioVision). Astrocyte and neuron apoptosis was analyzed via TUNEL staining using an *In Situ* Cell Death Detection Kit (11684817910, Roche). DAPI (300 nM) staining was used to visualize all cells.

Statistics

All data are presented as the mean ± SEM and were analyzed using IBM SPSS 20.0 software. The data were obtained from at least three replicates, and two-sided statistical tests were performed. Paired samples *t*-tests were used to analyze differences between paired groups.

Independent *t*-tests were used to analyze differences between two independent groups. One-way ANOVA was performed to analyze differences among multiple groups. Factorial analysis was performed to determine differences between groups at multiple time points. Repeated measures analysis was used to assess differences between groups in the neurobehavioral tests. Post hoc comparison was conducted according to the results of the test for equality of variance. $P < 0.05$ was considered to indicate significance.

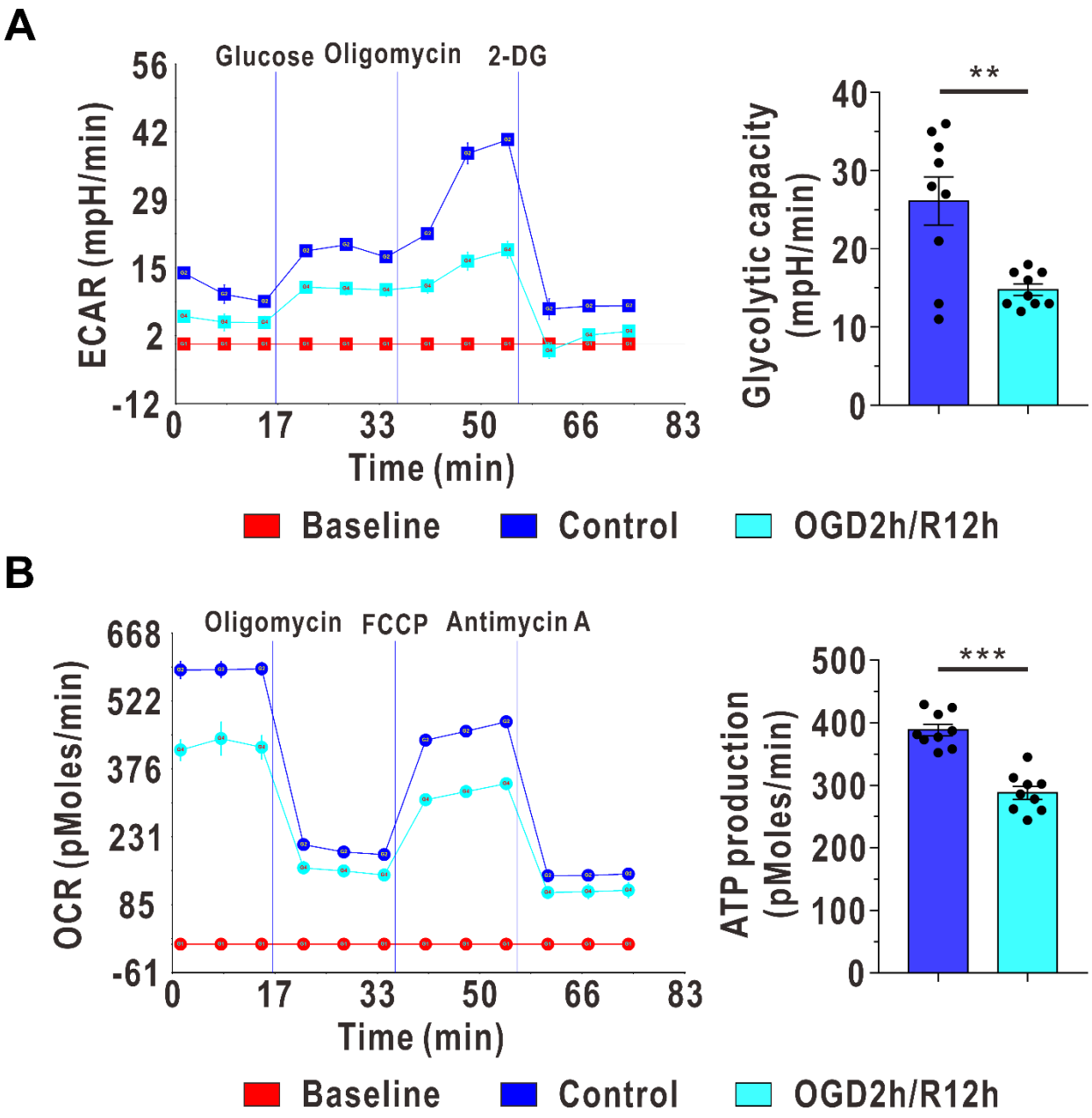

Figure S1. Astrocytic glycolytic capacity and ATP production during OGD/R insult in cultured astrocytes (related to Figure 1). (A) Left panel: Extracellular acidification rate (ECAR) at 12 h after reoxygenation. Right panel: The glycolytic capacity represents the maximum ECAR value after oligomycin injection (n = 9, independent t-test). (B) Left panel: Oxygen consumption rate (OCR) at 12 h after reoxygenation. Right panel: ATP production was

calculated by subtracting the OCR recorded in response to oligomycin from the baseline OCR recorded before the compounds were injected (n = 9, independent t-test). Data are presented as the mean ± SEM. $^{**}P < 0.01$. $^{***}P < 0.001$.

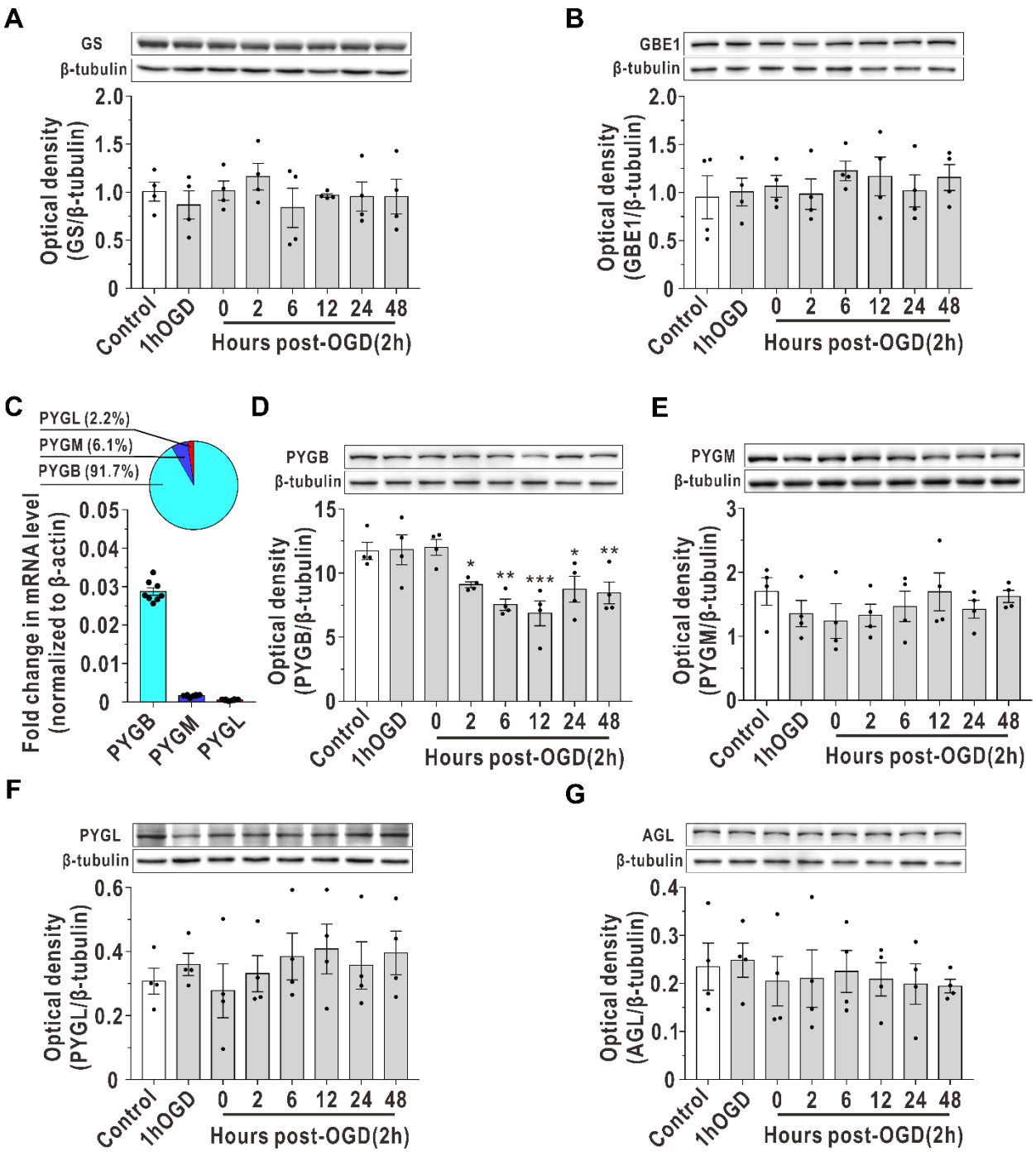

Figure S2. Expression of key enzymes in glycogenesis and glycogenolysis after OGD/R in cultured astrocytes (related to Figure 3). Protein levels of glycogen synthase (GS, A, one-way ANOVA with the Dunnett T3 multiple comparisons test) and glycogen branching enzyme (GBE1, B, one-way ANOVA with the LSD multiple comparisons test) after OGD/R in cultured

astrocytes, as measured by immunoblotting (n = 4). The relative optical density was calculated by dividing the density of the target band by that of the corresponding β-tubulin band. (C) The proportion of glycogen phosphorylase (GP) isoforms in cultured astrocytes (top panel) was determined based on the mRNA levels of the brain isoform of glycogen phosphorylase (PYGB), the muscle isoform of glycogen phosphorylase (PYGM) and the liver isoform of glycogen phosphorylase (PYGL), as measured by RT-qPCR (bottom panel, n = 8). The mRNA levels of PYGB, PYGM and PYGL were calculated as the fold change normalized to β-actin. (D-G) Protein levels of PYGB (D, one-way ANOVA with the LSD multiple comparisons test), PYGM (E, one-way ANOVA with the LSD multiple comparisons test), PYGL (F, one-way ANOVA with the LSD multiple comparisons test) and glycogen debranching enzyme (AGL, G, one-way ANOVA with the LSD multiple comparisons test) after OGD/R in cultured astrocytes (n = 4). Data are presented as the mean ± SEM. $^{*}P < 0.05$. $^{**}P < 0.01$. $^{***}P < 0.001$.

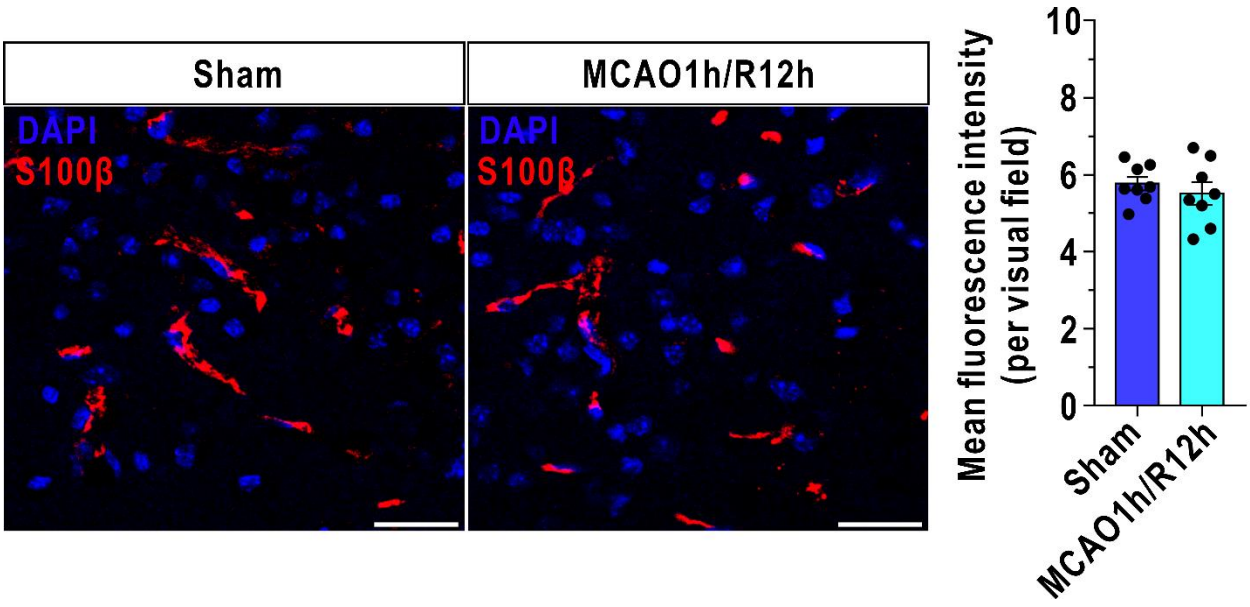

Figure S3. Fluorescence intensity of S100β after reperfusion in the mouse model of MCAO (related to Figure 4). Left panels: Coronal immunofluorescence images of frontal cortex area 1 in the ischemic penumbra after staining with an antibody against S100β. Right panels: Quantification of mean fluorescence intensity of S100β of the ischemic penumbra at 12 h after reperfusion (n = 8, independent t-test). Scale bars = 25 μm. The data are presented as the mean ± SEM.

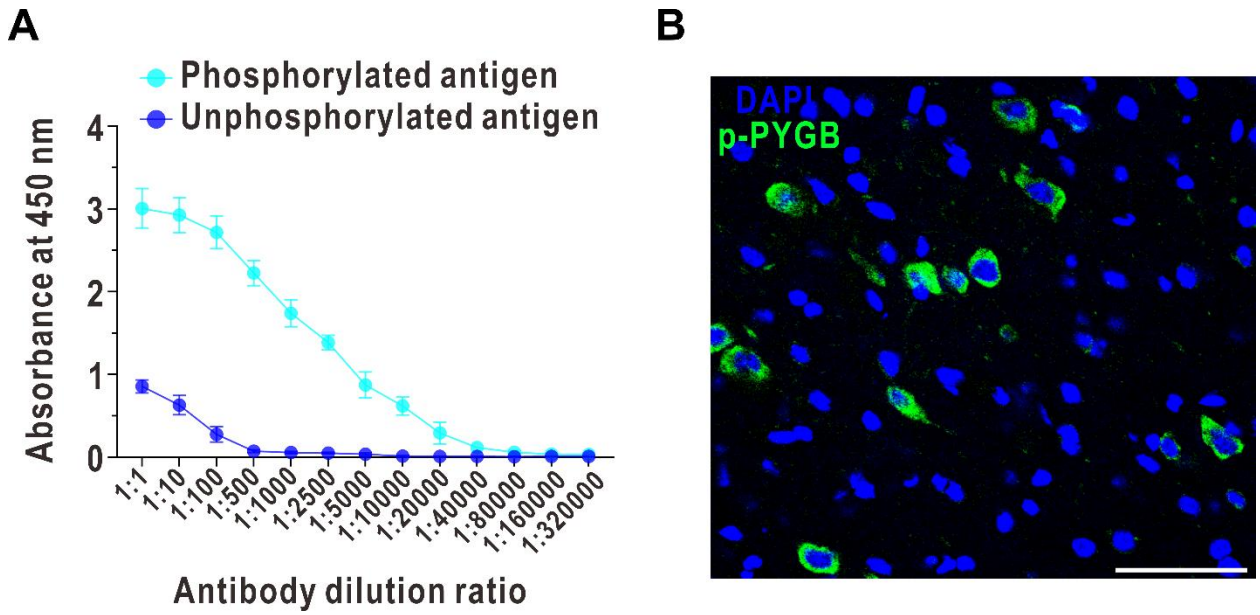

Figure S4. Identification of the phosphorylated PYGB antibody (related to Figure 4). (A) The absorbance at 450 nm of phosphorylated PYGB antibody towards phosphorylated antigen and unphosphorylated antigen using indirect ELISA with increasing dilution ratio (n = 3). (B) Recognition of phosphorylated PYGB (p-PYGB) by a phosphorylated PYGB antibody in mouse brain coronal slices from frontal cortex area 1 by immunofluorescence (dilution ratio is 1:500). Scale bar = 50 μm. The data are presented as the mean ± SEM.

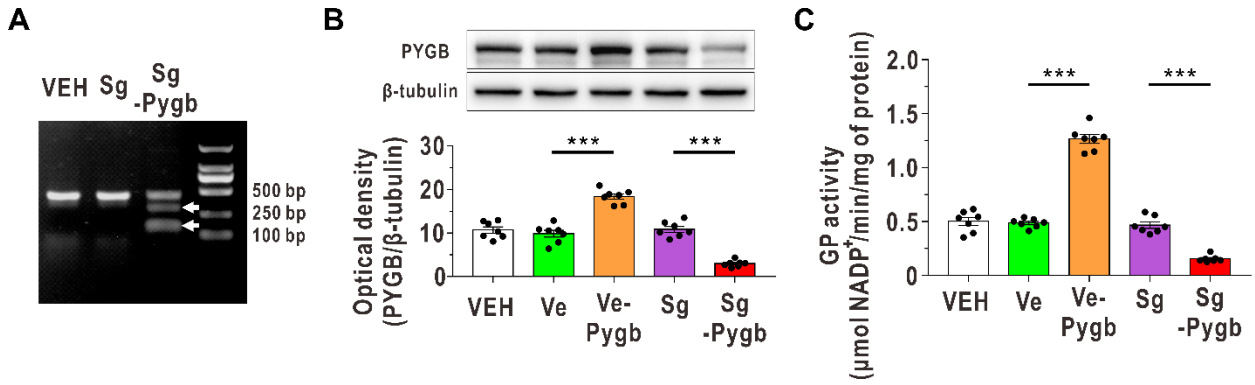

Figure S5. Verification of successful establishment of PYGB overexpression and CRISPR-Cas9 knockdown models in cultured astrocytes (related to Figure 5). (A) The astrocytic PYGB CRISPR-Cas9 knockdown model (named Sg-Pygb) was verified using a Knockdown and Mutation Detection Kit. VEH represents the vehicle group. Sg represents astrocytes infected with scrambled SgRNA lentiviruses. The arrows indicate the mutated DNA bands. (B) PYGB protein levels were determined in astrocytic PYGB overexpression (named Ve-Pygb) and knockdown models using immunoblotting (n = 7, one-way ANOVA with the LSD multiple comparisons test). Ve represents astrocytes infected with blank vector lentiviruses. (C) GP activity was analyzed in astrocytic PYGB overexpression and knockdown models (n = 7, one-way ANOVA with the LSD multiple comparisons test). The data are presented as the mean ± SEM. $^{***}P < 0.001$.

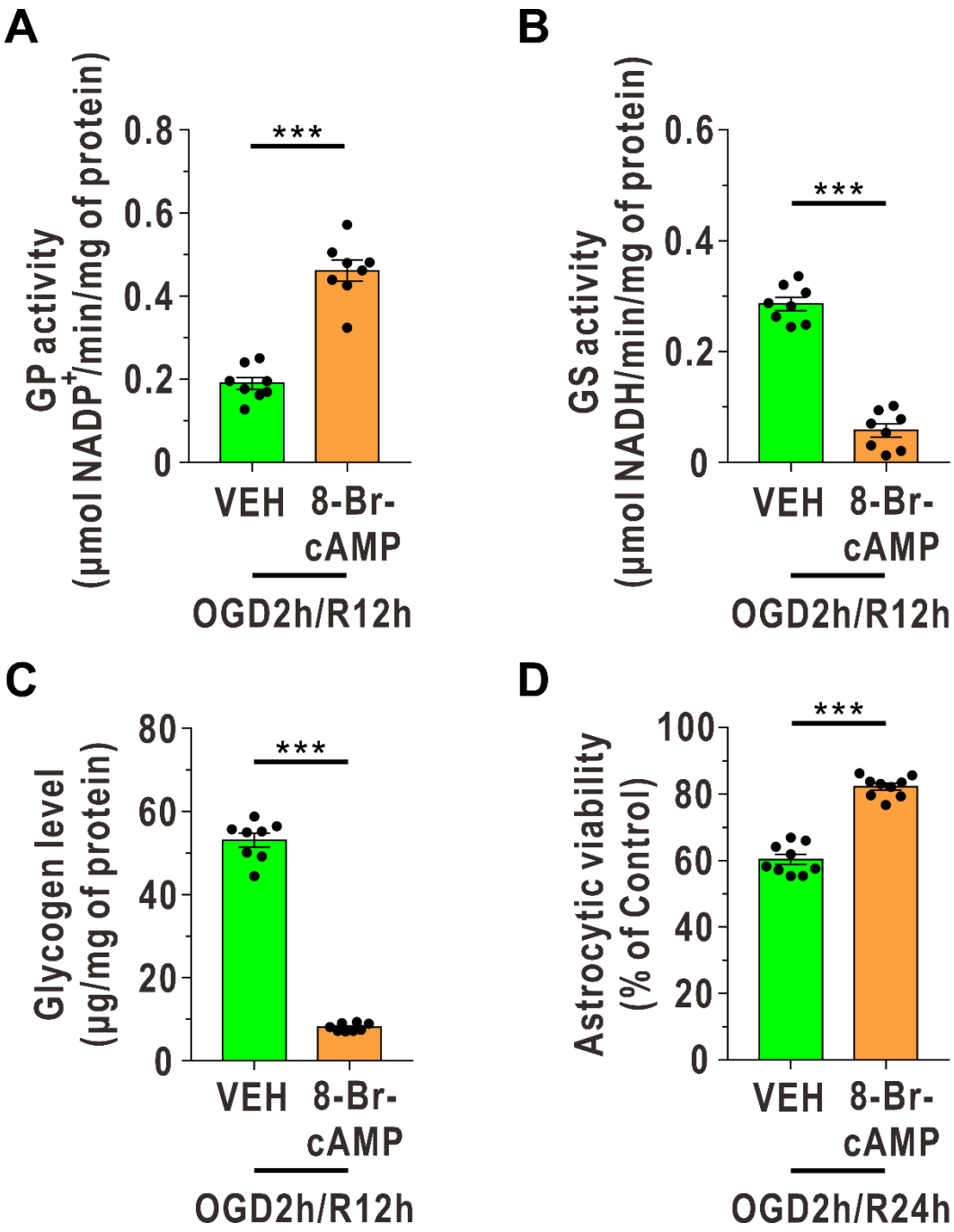

Figure S6. Pharmacological activation of GP improves the survival of cultured astrocytes after OGD/R treatment (related to Figure 5). (A and B) Quantified GP (A) and GS (B) activities in astrocytes treated with 8-Br-cAMP (a PKA agonist, 10 μM) at 12 h after reoxygenation (n = 8, independent t-test). 8-Br-cAMP was added to the cultured astrocytes at 2 h

after reoxygenation, and the treatment time was 10 h. VEH represents the vehicle group. (C) Glycogen levels in cultured astrocytes were quantified after 10 h of treatment with 8-Br-cAMP (n = 8, independent t-test). (D) Relative viability of 22-h 8-Br-cAMP-treated astrocytes at 24 h after OGD/R, as determined by a CCK-8 assay (n = 9, independent t-test). The data are presented as the mean ± SEM. $^{***}P < 0.001$.

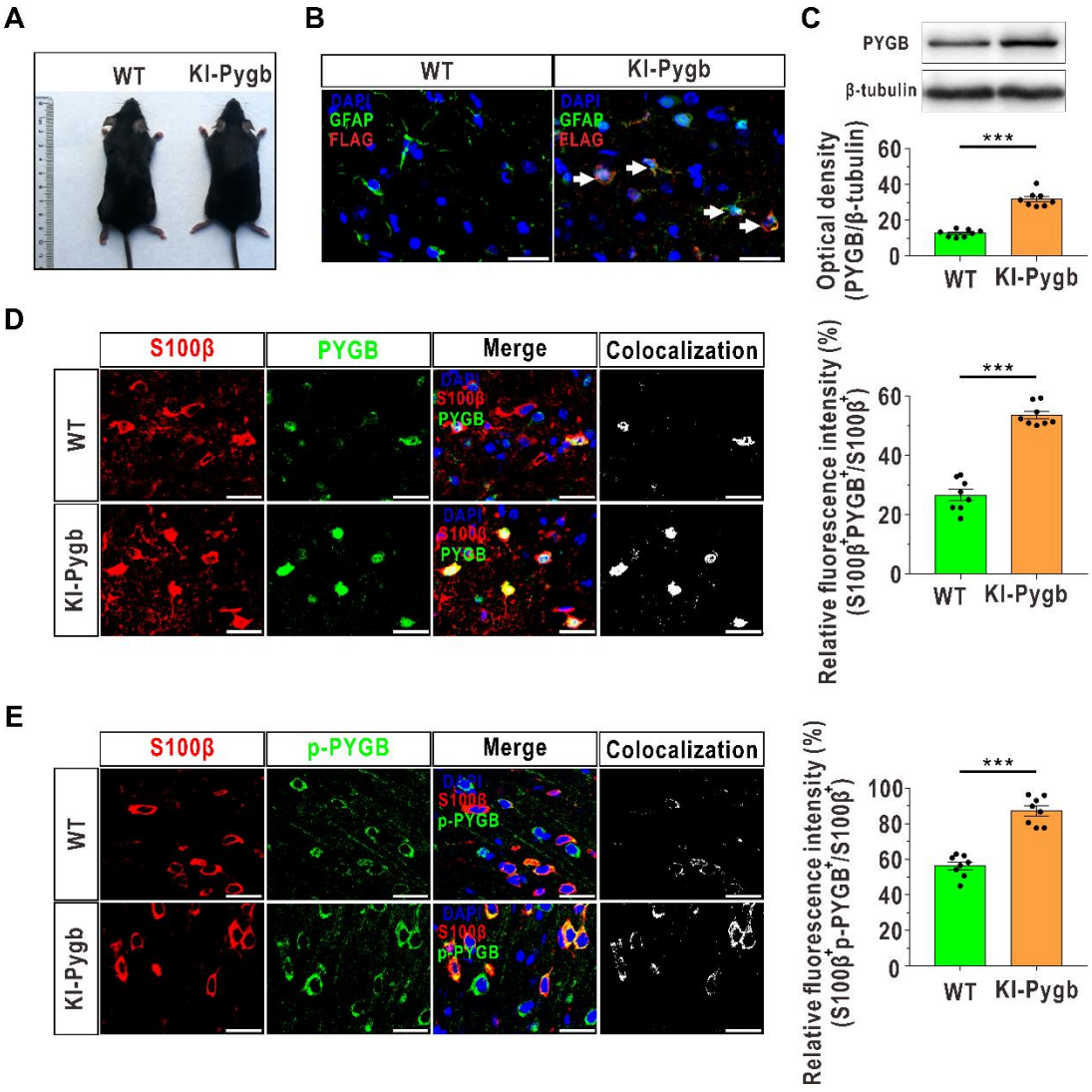

Figure S7. Verification of successful establishment of KI-Pygb mice (related to Figure 6).

(A) The appearance of KI-Pygb mice and WT littermate controls. (B) Immunofluorescence staining was performed to identify the astrocyte-specific localization of exogenous PYGB in knock-in mice. Astrocytes were marked by GFAP. The arrows represent astrocytes overexpressing the *pygb* gene followed by a FLAG tag. Scale bars = 25 μm. (C) The protein level of PYGB was analyzed by immunoblotting of lysates of frontal cortex area 1 in KI-Pygb mouse brains (n = 8, independent t-test). (D and E) Left panels: Representative immunofluorescence images after staining with an antibody against S100β and antibodies against

PYGB (D) and phosphorylated PYGB (p-PYGB, E) of frontal cortex area 1 in KI-Pygb mouse brains (n = 8, independent t-test). Right panels: Quantification of relative fluorescence intensity of PYGB (D) and p-PYGB (E). Astrocytes were marked with S100β. The relative fluorescence intensity of the target protein was calculated as the percentage of fluorescence intensity in the colocalization area (denoted as S100β and target protein) divided by the fluorescence intensity in the $S100\beta^{+}$ area. Scale bars = 25 μm. The data are presented as the mean ± SEM. $^{***}P < 0.001$.

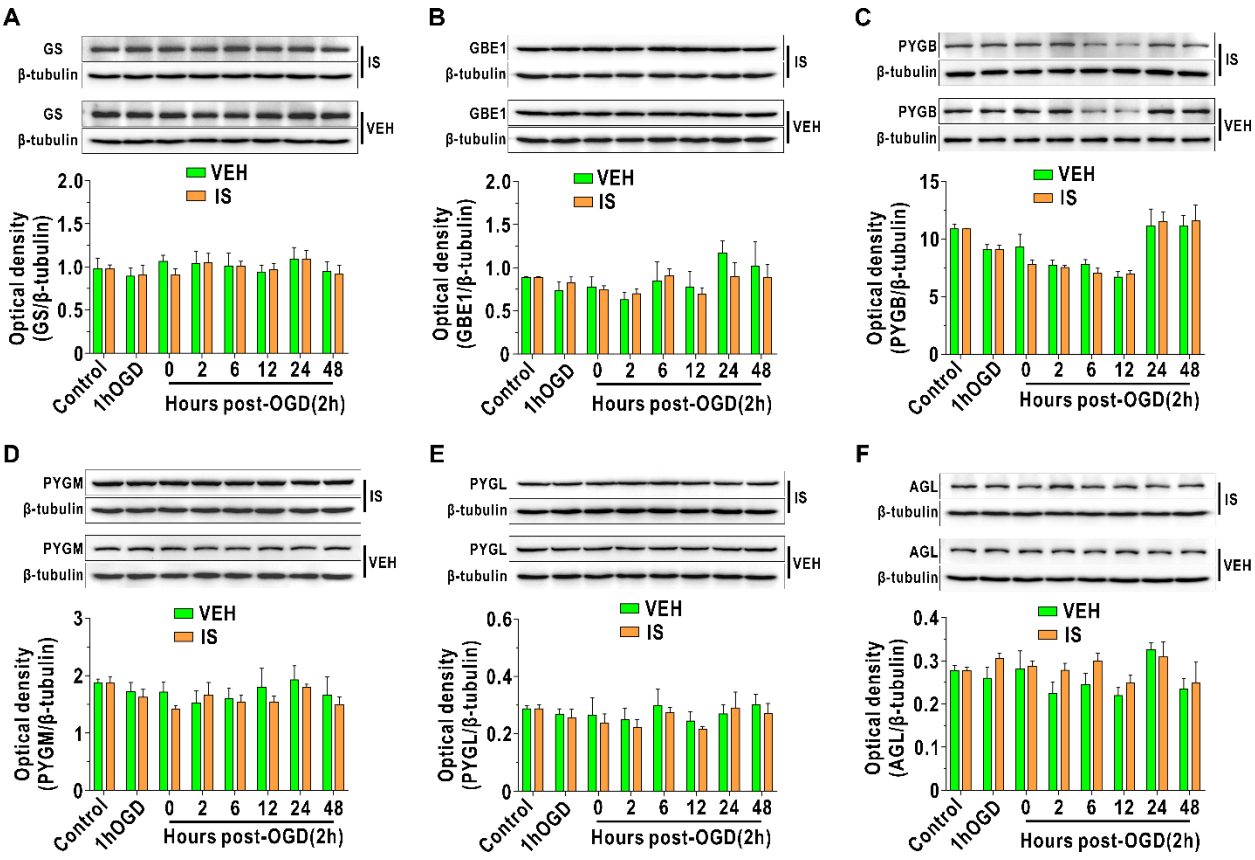

Figure S8. Expression of key enzymes in glycogen metabolism during OGD/R with insulin treatment in cultured astrocytes (related to Figure 7). Immunoblotting analysis was performed to assess the protein levels of GS (A), GBE1 (B), PYGB (C), PYGM (D), PYGL (E) and AGL (F) in cultured astrocytes treated with insulin (1 μM) after OGD/R (n = 4, factorial analysis). VEH represents the vehicle group, and IS represents the insulin group. Insulin was added to the medium immediately after reoxygenation. The data are presented as the mean ± SEM.

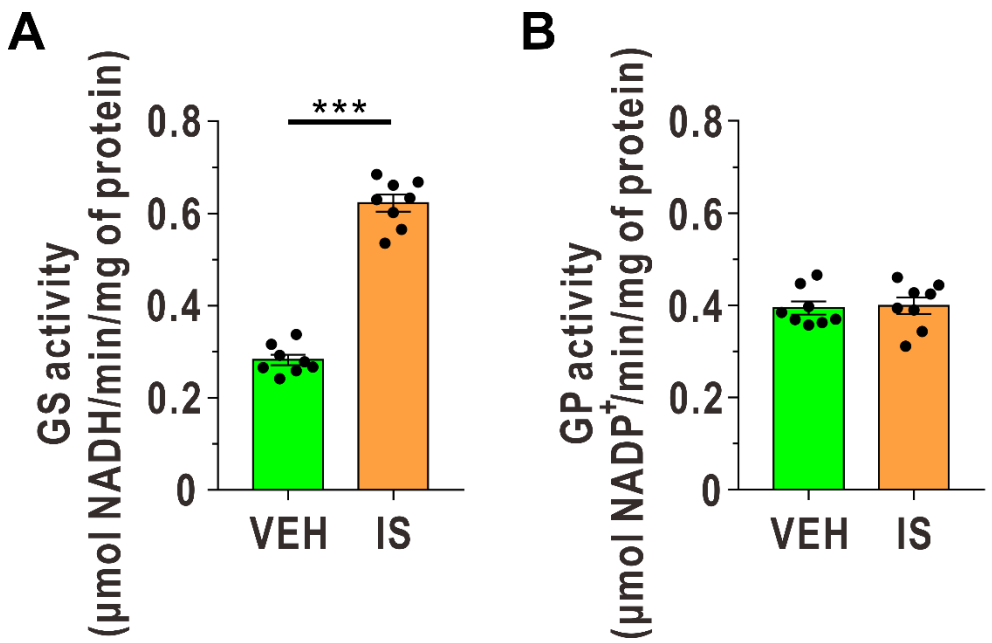

Figure S9. Insulin enhances GS activity but not GP activity in normal cultured astrocytes (related to Figure 7). (A and B) Quantified GS (A) and GP (B) activity in cultured astrocytes treated with insulin (1 μM, n = 8, independent t-test). VEH represents the vehicle group, and IS represents the insulin group. The incubation time for insulin with cultured astrocytes was 12 h. $^{***}P < 0.001$.

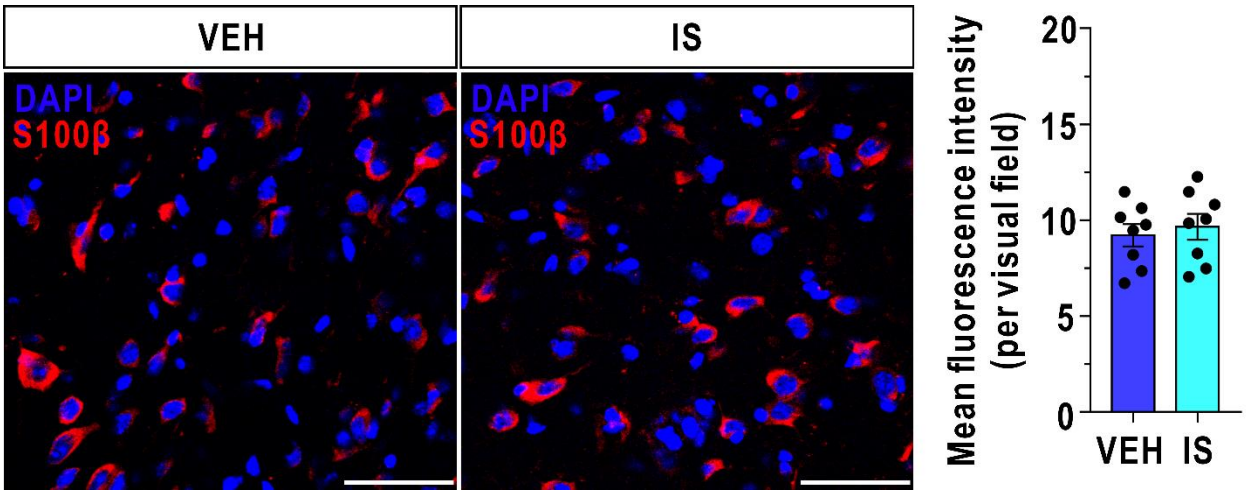

Figure S10. Fluorescence intensity of S100β with intracerebroventricular insulin (10 μM) treatment for 12 h (related to Figure 7). Left panels: Coronal immunofluorescence images of frontal cortex area 1 in insulin-treated mice after staining with an antibody against S100β. Right panels: Quantification of mean fluorescence intensity of S100β (n = 8, independent t-test). VEH represents the vehicle group, and IS represents the insulin group. Scale bars = 50 μm. The data are presented as the mean ± SEM.

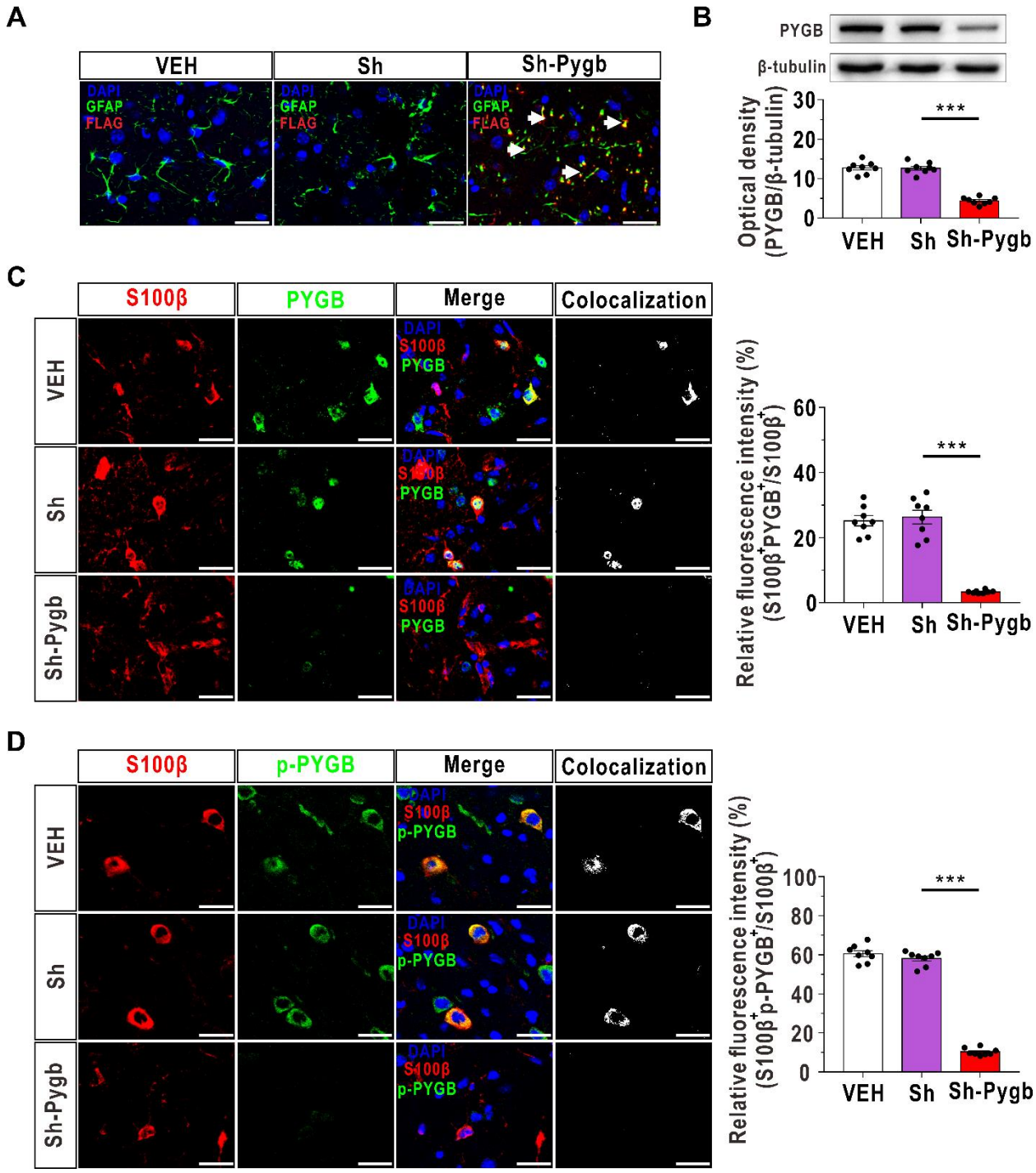

Figure S11. Verification of astrocyte-specific PYGB knockdown (Sh-Pygb) mice using AAVs containing the astrocytic promoter GFAP (related to Figure 8). (A) Immunofluorescence staining was performed to identify the astrocyte-specific localization of exogenous shRNA targeting PYGB in knockdown mice. Astrocytes were marked with GFAP.

The arrows represent PYGB-deficient astrocytes marked by a FLAG tag. VEH represents the vehicle group. Sh represents mice infected with scrambled shRNA AAVs. Scale bars = 25 μm. (B) The protein levels of PYGB were analyzed by immunoblotting of lysates of frontal cortex area 1 in Sh-Pygb mouse brains (n = 8, one-way ANOVA with the LSD multiple comparisons test). (C and D) Left panels: Representative immunofluorescence images after staining with an antibody against S100β and antibodies against PYGB (C) and phosphorylated PYGB (p-PYGB, D) of frontal cortex area 1 in Sh-Pygb mice (n = 8). Right panels: Quantification of relative fluorescence intensity of PYGB (C, one-way ANOVA with the LSD multiple comparisons test) and p-PYGB (D, one-way ANOVA with the Dunnett T3 multiple comparisons test). Astrocytes were marked with S100β. The relative fluorescence intensity of the target protein was calculated as the percentage of fluorescence intensity in the colocalization area (denoted as S100β and target protein) divided by the fluorescence intensity in the $S100\beta^{+}$ area. Scale bars = 25 μm. The data are presented as the mean ± SEM. $^{***}P < 0.001$.

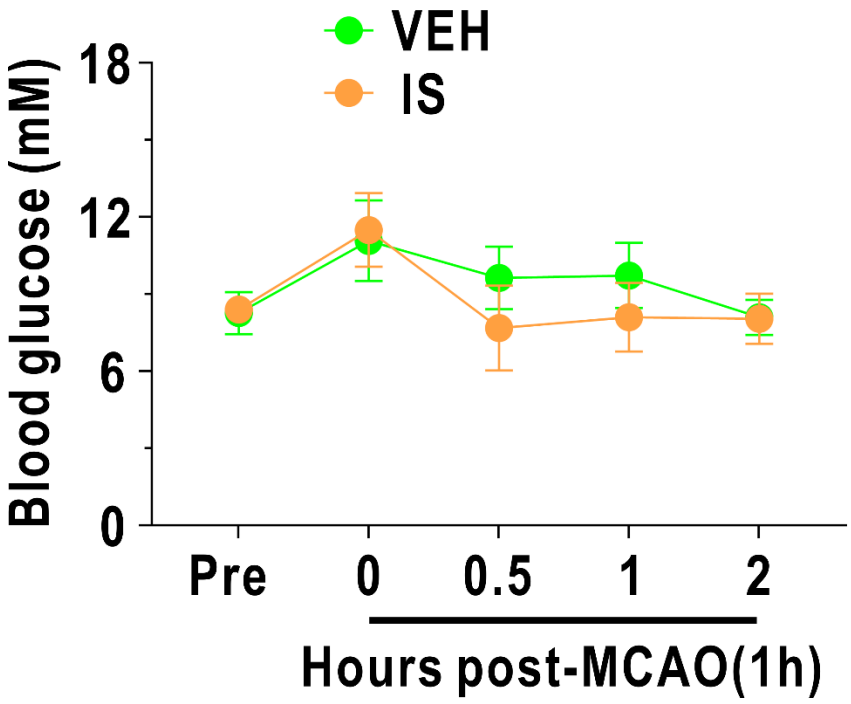

Figure S12. Intracerebroventricular injection of insulin does not affect blood glucose levels after MCAO/R (related to Figure 8). Blood glucose levels in mice subjected to insulin (10 μM) injection into the lateral ventricle immediately after reperfusion were tested using a blood glucose meter (vehicle: n = 6; insulin: n = 8, factorial analysis). VEH represents the vehicle group, and IS represents the insulin group. The data are presented as the mean ± SEM.

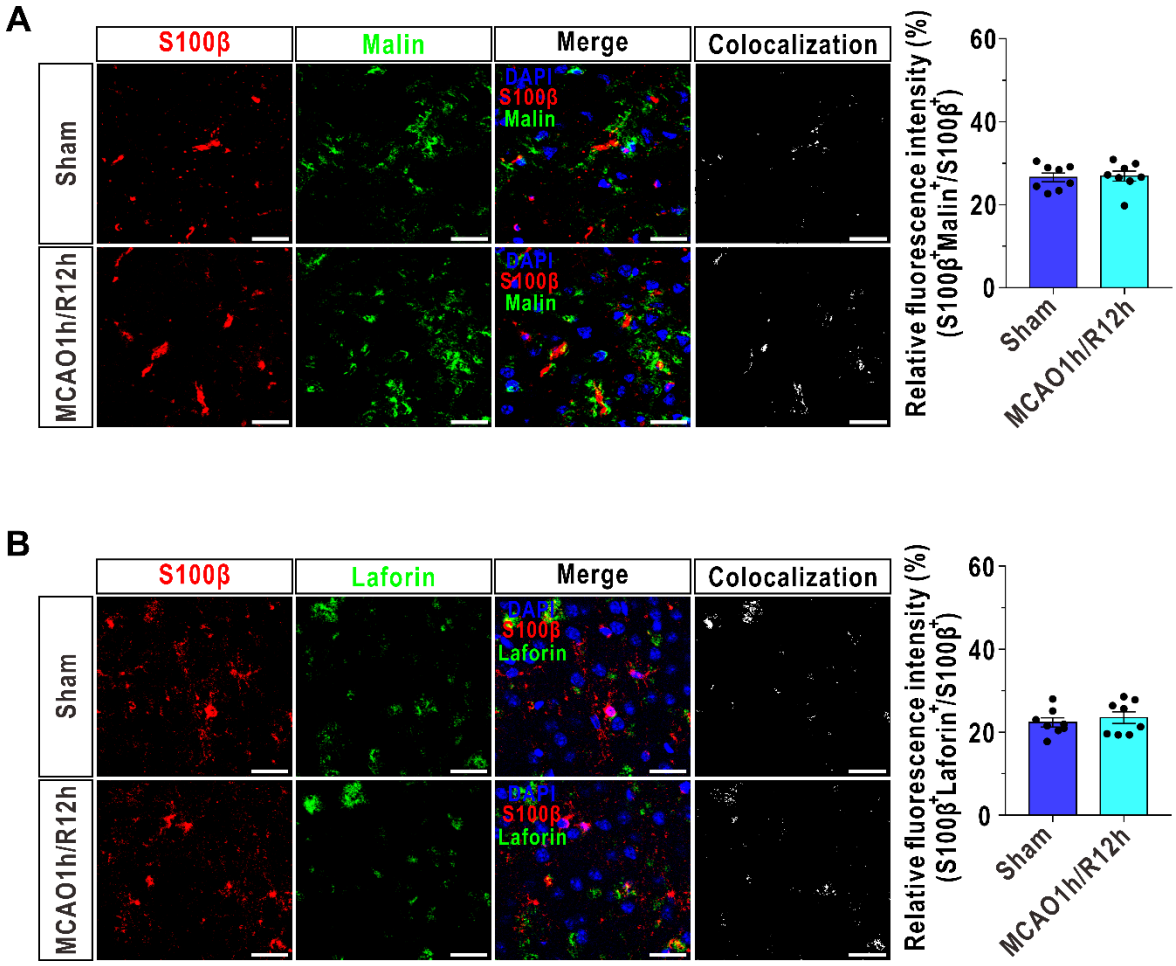

Figure S13. Protein levels of malin and laforin in astrocytes at 12 h after MCAO/R in mice (related to Figure 4). Left panels: Representative immunofluorescence images after staining with an antibody against S100β and antibodies against malin (A) and laforin (B) at 12 h after reperfusion in frontal cortex area 1 in the mouse model of MCAO (n = 8, independent t-test). Right panels: Quantification of relative fluorescence intensity of malin (A) and laforin (B) in astrocytes. The relative fluorescence intensity of the target protein was calculated as the percentage of fluorescence intensity in the colocalization area (denoted as S100β and target protein) divided by the fluorescence intensity in the $S100\beta^+$ area. Scale bars = 25 μm. The data are presented as the mean ± SEM.

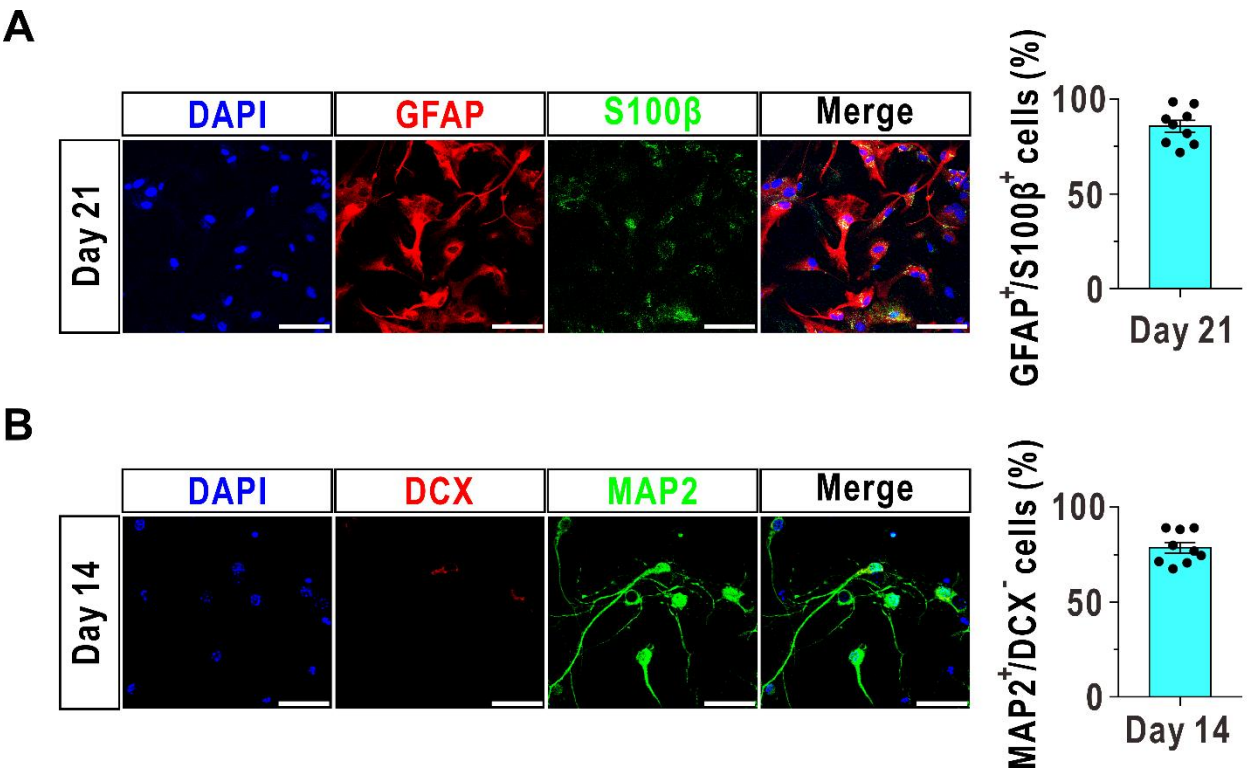

Figure S14. Evaluation of maturity in cultured astrocytes on day 21 and cultured neurons on day 14 (related to Figure 1). (A) Immunofluorescence staining was performed to evaluate the maturation of cultured astrocytes. Mature astrocytes were identified as $GFAP^+/S100\beta^+$ (n = 8). The percentage of $GFAP^+/S100\beta^+$ cells was calculated as the number of $GFAP^+/S100\beta^+$ cells divided by the total cells marked by DAPI. Scale bars = 50 μm. (B) Immunofluorescence staining was performed to evaluate the maturation of cultured neurons (n = 8). Mature neurons were identified as $MAP2^+/DCX^-$. The percentage of $MAP2^+/DCX^-$ cells was calculated as the number of $MAP2^+/DCX^-$ cells divided by the total cells marked by DAPI. Scale bars = 50 μm. The data are presented as the mean ± SEM.

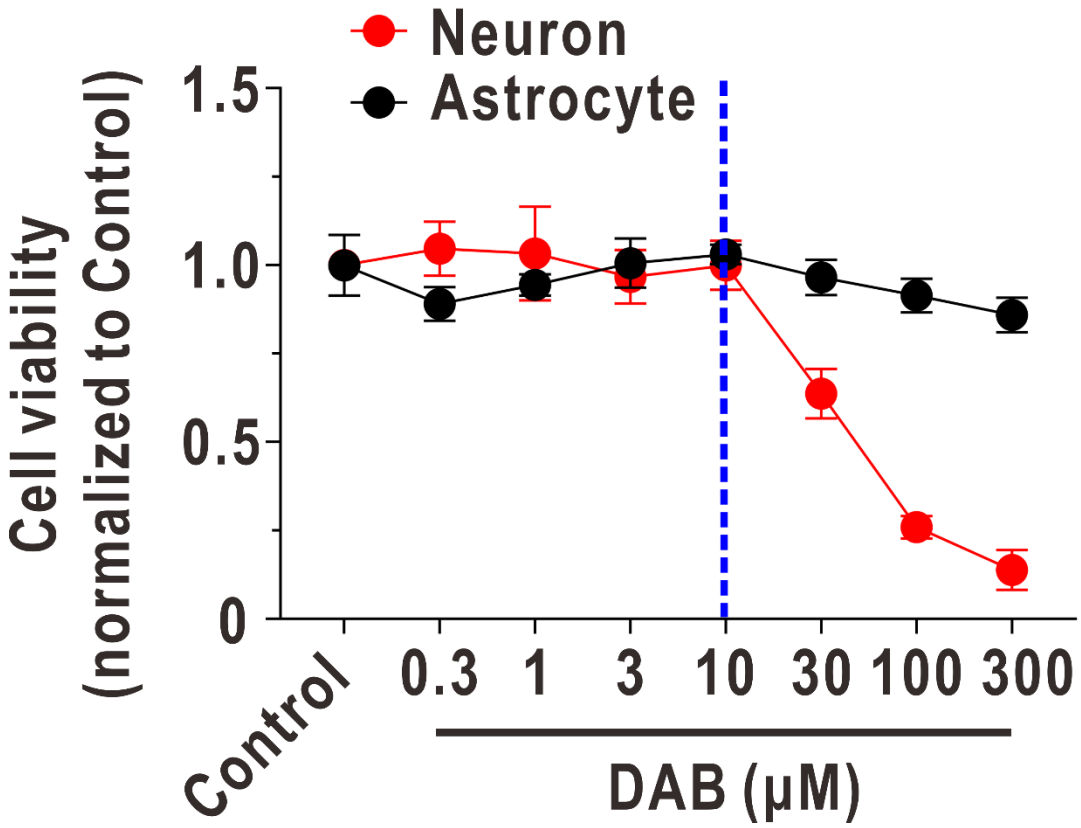

Figure S15. The cell viability of cultured astrocytes and neurons treated with increasing doses of DAB for 24 h (related to Figure 5). The cell viabilities of cultured astrocytes and neurons were determined by CCK-8 and normalized to the control group (n = 4). Neurons showed higher sensitivity than astrocytes to DAB. When DAB was over 10 μM, it exerted cytotoxic effects on cultured neurons. The data are presented as the mean ± SEM.

Table S1. Demographics of the included stroke patients (related to Figure 1).

Sample ID	Age	Sex	PMI (min)	Infarction region	Interval from thrombolysis to death (h)
2016CBB0020	88	Male	37	Left temporal lobe	13
2016CBB0022	79	Male	42	Left temporal lobe, left frontal lobe	12.5
2017CBB020	78	Male	34	Left temporal lobe, left frontal lobe, left parietal lobe	11
2016CBB0031	95	Male	36	Left temporal lobe	14

PMI: postmortem interval.

Table S2. Sources of the antibodies used in this study (related to Figure 4, 6 and 7).

Target of antibody	Source	Application	Dilution	Identifier
PYGB	Abcam	IB	1:1000	ab154969
PYGB	Atlas Antibodies	IF	1:100	HPA031067
PYGM	Abcam	IB	1:1000	ab81901
PYGM	Abcam	IF	1:100	ab231963
PYGL	Proteintech Group	IB, IF	1:500, 1:100	15851-1-AP
GS	Abcam	IB, IF	1:1000, 1:200	ab40867
GBE1	Proteintech Group	IB, IF	1:1000, 1:50	20313-1-AP
AGL	AgriSera	IB	1:1000	AS09 454
AGL	Abcam	IF	1:100	ab133720
Phosphorylated GS (Ser641)	Cell Signaling Technology	IF	1:200	47043
Phosphorylated PKA (Ser338/Thr197)	Cell Signaling Technology	IF	1:200	9621
Phosphorylated GSK3β (Ser9)	GeneTex	IF	1:150	GTX50090
β-tubulin	Cell Signaling Technology	IB	1:1000	2128
GFAP	Abcam	IF	1:50	ab4648
S100β	Abcam	IF	1:200	ab52642
MAP2	Abcam	IF	1:500	ab11267
FLAG tag	Cell Signaling Technology	IF	1:800	14793
DCX	Abcam	IF	1:250	ab207175

Malin	GeneTex	IF	1:100	GTX32750
Laforin	Abcam	IF	1:200	ab129321
Mouse IgG H&L (Fluor 488)	Thermo Fisher Scientific	IF	1:500	A-11029
Mouse IgG H&L (Fluor 594)	Thermo Fisher Scientific	IF	1:500	A32742
Rabbit IgG H&L (Fluor 488)	Thermo Fisher Scientific	IF	1:500	A32731
Rabbit IgG H&L (Fluor 594)	Thermo Fisher Scientific	IF	1:500	R37117
Rabbit IgG H&L (HRP)	Abcam	IB	1:5000	ab6721
Mouse IgG H&L (HRP)	Abcam	IB	1:5000	ab6789
Phosphorylated PYGB (Ser14)	Gene Create Biotech	IF	1:500	Customized antibody

IB: immunoblotting; IF: immunofluorescence.

Table S3. Sequences of the primers used for RT-qPCR (related to Figure 3 and 5).

Gene	Primer
gs *(GenBank: NM_030678)*	Forward: 5′- TCAGAGCAAAGCACGAATCCAG -3′ Reverse: 5′- CATAGCGGCCAGCGATAAAGA -3′
gbe1 *(GenBank: NM_028803)*	Forward: 5′- ACTACCGAGTCGGGACAGCAA -3′ Reverse: 5′- GGTCCAGTCTCTGATGACCTCCATA -3′
pygb *(GenBank: NM_153781)*	Forward: 5′- TGCAGACTATGAAGCCTACATCCA -3′ Reverse: 5′- AGAACTTGCCAGAGCAGGCTATATT -3′
pygm *(GenBank: NM_011224)*	Forward: 5′- TCAACTGCCTGCACATCATCAC -3′ Reverse: 5′- CATGATAGTCCTCGGCACCATAAAC -3′
pygl *(GenBank: NM_133198)*	Forward: 5′- ACCTCTGTGGCAGAAGTGGTGA -3′ Reverse: 5′- CCGATAGGTCTGTGGCTGGAA -3′
agl *(GenBank: NM_001081326)*	Forward: 5′- ACTGTGGCACGTGGATGGATAA -3′ Reverse: 5′- CCCACGATTTCCACAGCAGA -3′
β-actin	Forward: 5′- CTTCTTTGCAGCTCCTTCGTTG -3′ Reverse: 5′- ATGGAGGGGAATACAGCCCG -3′

REFERENCES

Atangana, E.N., Homburg, D., Vajkoczy, P., and Schneider, U.C. (2015). Mouse cerebral magnetic resonance imaging fails to visualize brain volume changes after experimental subarachnoid hemorrhage. Acta Neurochir. 157, 37–42.

Bergmann, S.M., Wang, Q., Zeng, W., Li, Y., Wang, Y., Matras, M., Reichert, M., Fichtner, D., Lenk, M., Morin, T., et al. (2017). Validation of a KHV antibody enzyme-linked immunosorbent assay (ELISA). J Fish Dis 40, 1511-1527.

Brenner, M., Kisseberth, W.C., Su, Y., Besnard, F., and Messing, A. (1994). GFAP promoter directs astrocyte-specific expression in transgenic mice. J. Neurosci. 14, 1030–1037.

Chen, Z., Hu, Q., Xie, Q., Wu, S., Pang, Q., Liu, M., Zhao, Y., Tu, F., Liu, C., and Chen, X. (2019). Effects of treadmill exercise on motor and cognitive function recovery of MCAO mice through the Caveolin-1/VEGF signaling pathway in ischemic penumbra. Neurochem. Res. 44, 930–946.

Cho, J.-H., Kim, A.H., Lee, S., Lee, Y., Lee, W.J., Chang, S.-C., and Lee, J. (2018). Sensitive neurotoxicity assessment of bisphenol A using double immunocytochemistry of DCX and MAP2. Arch. Pharm. Res. 41, 1098–1107.

Li, L., and Zuo, Z. (2011). Glutamate transporter type 3 knockout reduces brain tolerance to focal brain ischemia in mice. J. Cereb. Blood Flow Metab. 31, 1283–1292.

Raponi, E., Agenes, F., Delphin, C., Assard, N., Baudier, J., Legraverend, C., and Deloulme, J.-C. (2007). S100B expression defines a state in which GFAP-expressing cells lose their neural stem cell potential and acquire a more mature developmental stage. Glia 55, 165-

177.

Šakić, B. (2019). Cerebrospinal fluid collection in laboratory mice: Literature review and modified cisternal puncture method. J. Neurosci. Methods 311, 402–407.

Walls, A.B., Sickmann, H.M., Brown, A., Bouman, S.D., Ransom, B., Schousboe, A., and Waagepetersen, H.S. (2008). Characterization of 1,4-dideoxy-1,4-imino-d-arabinitol (DAB) as an inhibitor of brain glycogen shunt activity. J Neurochem 105, 1462-1470.

Wu, D., Chandra, A., Chen, J., Ding, Y., and Ji, X. (2018). Endovascular Ischemic Stroke Models in Nonhuman Primates. Neurotherapeutics 15, 146-155.

Zhang, L., Schallert, T., Zhang, Z.G., Jiang, Q., Arniego, P., Li, Q., Lu, M., and Chopp, M. (2002). A test for detecting long-term sensorimotor dysfunction in the mouse after focal cerebral ischemia. J. Neurosci. Methods 117, 207–214.